The effect of vehicle parameter variation on drift equilibria points

MSc. Thesis

J.J.A. Kramer

TU Delft

The effect of vehicle parameter variation on drift equilibria points

MSc. Thesis

by

J.J.A. Kramer

to obtain the degree of
Master of Science
in Mechanical Engineering
Track: Vehicle Engineering
Specialization: Dynamics & Control

at the Delft University of Technology

Student number: 4330013

Thesis committee:

Dr. ir. J.C.F. de Winter,	TU Delft, Chair, CoR
Dr. B. Shyrokau,	TU Delft, Supervisor, CoR
A. Bertipaglia,	TU Delft, CoR

An electronic version of this thesis is available at
http://repository.tudelft.nl/.

TU Delft

Acknowledgements

I would like to take a brief moment to thank the people that have helped me with feedback and support. Without them I would have never finished this thesis. First, I would like to thank Barys Shyrokau for supervising me on this thesis. Futhermore, I would like to thank Joost de Winter and Alberto Bertipaglia for evaluating my work by being part of the thesis committee.

Additionally I would like to thank my friends and family for their patience and for providing me with an endless source of comfort and motivation.

Jelle Kramer
Delft, August 22, 2022

“*Luctor et Emergo*”

Abstract

A vehicle that is travelling at high sideslip angles can still be controlled by drifting. Implemented into a vehicle, this phenomenon could lead to increased vehicle safety and performance. Additionally, it could lead to higher acceptance rates of autonomous driving.
In this work a three state vehicle model is used. Using this model, simulations are performed with varying vehicle parameters and tyre models. First, the mathematical descriptions of all used models are stated, after which phase plane representations for the identification of drift equilibria are elaborated on. Next, different steering characteristics and their influence on the drift equilibrium points are considered. These characteristics are achieved by varying the lateral rear tyre stiffness. The effect of three different types of tyre models on the drift equilibria is discussed. The models that are considered are the linear tyre model, Dugoff tyre model and Magic Formula model.
In addition to this, the effects of the location of the centre of gravity, the vehicle mass and the cornering stiffness are investigated. Finally the outcome of the Dugoff tyre model and the Magic Formula model for construction of drift equilibria is shown and discussed.
Contrary to the Dugoff and Magic Formula model, no drift equilibria were found using the linear tyre model. Using the Dugoff model, drift equilibrium points were found for the understeering and neutral steering vehicle, whereas the oversteering vehicle showed drift equilibrium ranges. Finally, drift equilibria depend on vehicle parameters, showing change in behaviour when the latter are varied.

Contents

Acknowledgements iii

Abstract vii

1 Introduction 1
- 1.1 Background . . . 1
- 1.2 Research Relevance and State of the Art . . . 2
  - 1.2.1 Acceptance . . . 2
  - 1.2.2 Safety . . . 3
  - 1.2.3 Performance . . . 6
- 1.3 Problem definition . . . 8
- 1.4 Contributions . . . 8
- 1.5 Thesis Layout . . . 8

2 Vehicle Modelling 9
- 2.1 Vehicle Model . . . 9
  - 2.1.1 Bicycle Model . . . 9
- 2.2 Tyre Model . . . 10
  - 2.2.1 Linear Tyre Model . . . 11
  - 2.2.2 Dugoff Tyre Model . . . 11
  - 2.2.3 Pacejka Tyre Model (Magic Formula) . . . 11
  - 2.2.4 Wheel dynamics . . . 12
- 2.3 Tyre forces . . . 13
- 2.4 Summary . . . 14

3 Stability analysis 15
- 3.1 Phase Plane . . . 15
  - 3.1.1 High sideslip manoeuvring . . . 15
  - 3.1.2 Steady state solution . . . 17
- 3.2 Different steering characteristics . . . 18
  - 3.2.1 Understeer . . . 20
  - 3.2.2 Neutral Steer . . . 20
  - 3.2.3 Oversteer . . . 21
- 3.3 Different Tyre Models . . . 22
  - 3.3.1 Linear Tyre Model . . . 22
  - 3.3.2 Dugoff Tyre Model . . . 22
  - 3.3.3 Pacejka Tyre Model (Magic Formula) . . . 23
- 3.4 Summary . . . 23

4 Drift equilibria 25
- 4.1 Varying Vehicle Parameters . . . 26
  - 4.1.1 Vehicle Geometry . . . 26
  - 4.1.2 Vehicle Mass . . . 27
  - 4.1.3 Cornering Stiffness . . . 28
- 4.2 Varying Tyre Model . . . 30
- 4.3 Summary . . . 31

5 Conclusions & Recommendations 33
- 5.1 Conclusions . . . 33
- 5.2 Recommendations . . . 34

A Appendix A: Parameters 37

List of Figures

1.1 Volkswagen Polo WRC in a drifting motion during the World Rally Championship [18]. . 1
1.2 SAE level 4 concept car interior design [9]. Here drivers might not even face forward. . 2
1.3 Trajectory of a rear-wheel drive vehicle during stabilization [32]. 3
1.4 Driver input data and vehicle states [32]. 4
1.5 A T-bone collision [25]. 4
1.6 Decision making options for different velocities and longitudinal distances between the vehicle and an obstacle. [8]. 5
1.7 The obstacle is successfully avoided by the vehicle using clothoid based manoeuvres. [15]. 6
1.8 Actual trajectory and velocity of the vehicle during the experiment [15]. 7
1.9 Vehicle trajectories for maximum exit velocity at different road surfaces [30]. 7

2.1 A vehicle taking a right hand side corner [33] 9
2.2 Bicycle model [33]. 10
2.3 $X - Y$ curve produced by the original Magic Formula [21]. 12
2.4 Tyre forces for the Linear Tyre Model, Dugoff Tyre Model and Magic Formula Model. . . 14

3.1 Visualization of typical cornering (left) and drift (right) vehicle motion [17]. 16
3.2 Example of a phase plane representation. Three equilibria, depicted by red dots, are visible. The middle equilibrium is stable and corresponds to conventional cornering. The other two are unstable high-sideslip equilibria. 17
3.3 Grid of initial conditions for vehicle sideslip angle β and yaw rate r. 18
3.4 Visualization of oversteer, neutral steer and understeer vehicle steering characteristics with increasing vehicle velocity on a curvature of $R = 30$m. 19
3.5 Steady state solution for drift equilibria, using Dugoff tyre model and understeering characteristics, visualized in a phase plane diagram. 20
3.6 Steady state solution for drift equilibria, using Dugoff tyre model and a neutral steering behaviour, visualized in a phase plane diagram. 21
3.7 Steady state solution for drift equilibria, using Dugoff tyre model and oversteering characteristics, visualized in a phase plane diagram. 21
3.8 Steady state solution for drift equilibria, using Linear tyre model and a neutral steering behaviour with initial conditions as shown in Figure 3.3, visualized in a phase plane diagram. 22
3.9 Steady state solution for drift equilibria, using Magic Formula model and a neutral steering behaviour, visualized in a phase plane diagram. 23

4.1 Drift equilibria results for the vehicle parameterized by Table A.1, with varying location of the centre of gravity. 27
4.2 Drift equilibria results for the vehicle parameterized by Table A.1, with varying vehicle mass. 28
4.3 Drift equilibria results for the vehicle parameterized by Table A.1, with varying cornering stiffnesses. 29
4.4 Drift equilibria results for the vehicle parameterized by Table A.1, for Dugoff tyre model and Magic Formula model. 30

List of Tables

1.1 The three case descriptions [8]. 5
1.2 Option windows for the three cases [8]. 5
1.3 Recommended actions for the three considered cases [8]. 5

A.1 Vehicle and road parameters used to create the phase plane representation shown in Figure 3.6. The vehicle values are of a Porsche 911, extracted from IPG Carmaker [33]. 37
A.2 Pacejka tyre model parameters for a tyre with non-convex slip properties as used in [33]. 37

List of Symbols

α	Lateral slip angle
β	Vehicle sideslip angle
$\dot{\beta}$	Sideslip angle rate
δ	Steering angle
κ	Longitudinal slip
κ_t	Trajectory curve
λ	Dugoff weighting coefficient
μ	Road friction coefficient
μ_0	Peak road friction coefficient
ω	Angular wheel velocity
σ	Theoretical slip quantity
$a, \dot{v}$	Acceleration
B	Stiffness factor
C	Shape factor
C_α	Lateral tyre stiffness
C_κ	Longitudinal tyre stiffness
D	Peak value
E	Curvature factor
e_r	Friction reduction coefficient
F	Force
g	Gravitational acceleration
I_ω	Wheel inertia
I_z	Yaw inertia
K_{us}	Understeer gradient
l	Distance between CoG and axle
L	Vehicle length
m	Vehicle mass
M_z	Yaw moment
r	Yaw rate
$\dot{r}$	Yaw acceleration
R	Corner radius
r_ω	Effective wheel radius
S	Shift
T_{net}	Net rear axle torque
V, v, u	Vehicle velocity

Subscripts

f	Front
h	Horizontal
r	Rear
v	Vertical
x	Longitudinal
y	Lateral
z	Normal

1 Introduction

1.1. Background

To assist the driver of a vehicle in its driving task, advanced driver assistance systems (ADAS) are developed. The complexity and capability of (combinations of) these systems are distinguishable by their SAE levels, ranging from SAE level 1 to SAE level 5 [24]. Examples of SAE level 1 systems are Lane Departure Warning (LDW) and Lane Keeping Assistance Systems (LKAS) as they can be easily overridden by the inputs of the driver. The operating envelope of second level SAE systems is limited to regular motorway driving conditions in which the longitudinal and lateral dynamics are not fully excited simultaneously. However, as the long term goal for automotive development is to reach full autonomy (SAE level 5), a vehicle should be able to drive on its own in all conditions, even the most severe ones. Therefore research is now performed to open and expand the path towards full vehicle autonomy.

A vehicle that drives at large sideslip angles has not necessarily lost all control. Properly controlled, this type of driving, called drifting, can even increase vehicle safety. During a drifting manoeuvre, shown in Figure 1.1, a vehicle operates at its handling limits as the tyres are saturated [17].

Figure 1.1: Volkswagen Polo WRC in a drifting motion during the World Rally Championship [18].

On loose and low friction surfaces large sideslip angles result in an increase in lateral acceleration. However, a drifting motion is highly unstable. Therefore, a drifting manoeuvre can only be handled by high-skilled drivers. Rally drivers, who often drive on low friction surfaces, utilize this technique to minimize cornering time. Thanks to current systems vehicles can already perform the driving task safely on tarmac [3]. To increase vehicle safety on loose surfaces it would be beneficial to reproduce the advanced skills performed by rally drivers on autonomous vehicles.

Maximum lateral acceleration on tarmac is achieved at low sideslip angles [3]. However, on loose surfaces the shape of the friction-slip diagram changes. Therefore, in contrast to cornering on tarmac, maximum lateral acceleration is achieved at high sideslip angles. Comparing conventional cornering (low sideslip angles) to drifting it becomes clear that that a higher lateral acceleration can be achieved using the latter driving technique [17].

Current systems like Electronic Stability Control (ESC) focus on limiting sideslip angles to low values. These systems are not designed for drifting. To increase vehicle safety, control opportunities that rely on rear tyre saturation rather than avoiding it can also be considered [17]. Investigation of this type of control opportunities within the context of autonomous car development can lead to a broader perspective on future systems for vehicle safety and performance enhancement.

Control algorithms for autonomous and semi-autonomous vehicles that utilize rear tyre saturation manoeuvres for the purpose of collision mitigation and avoidance have already been investigated. Literature shows a control technique that mitigates the severity of a side collision, where vehicles travel in perpendicular directions, by deliberately saturating the rear tyres and thereby rapidly re-orientating one of the vehicles [8]. In another research an obstacle avoidance algorithm was developed that incorporated drifting as one of the allowable operating conditions for a vehicle to solve otherwise infeasible obstacle avoidance problems [15]. In both of these researches, practical applications for rear tyre saturation cornering are presented. The safety benefits that come with vehicle assistance systems that perform on the same skill level as professional racing drivers, should not be underestimated.

1.2. Research Relevance and State of the Art

In current research, several reasons are brought up on why and how autonomous drifting can be beneficial for improvement of vehicles.

1.2.1. Acceptance

The phenomenon of autonomous vehicles is still not widely accepted by the main public [19]. This is despite the investments made on technology for autonomous vehicles [20]. With the increase of autonomy, the safety perceived by the users is reduced [16]. Furthermore, the low acceptance rates are caused by loss of driving enjoyment, which is typically offered by premium luxury brands, with increasing autonomy of the vehicle. In order to increase the popularity of self-driving vehicles, it is therefore expected that the development of advanced driving systems is of vital importance [2]. More precisely, these should be driving systems that can exhibit driving features that can normally only be performed by highly skilled drivers.

When searching particularly for the acceptance of autonomous drifting itself, no specific research has been found. However, research has been performed on the acceptance on other driver assistance systems [13] and on the overall acceptance of autonomous vehicles by users [10]. The acceptance of the autonomous vehicle as a whole has been researched as well [10]. Automated vehicles from SAE level 4 [24] and above are envisioned to, at least for a while, drive to the assigned destination autonomously. As a result the driver can perform non-driving related activities [23]. Therefore autonomous vehicle interior design and even seating plan will change accordingly, shown in Figure 1.2. Acceptance of such interior designs in combination with advanced driving assistance systems is yet to be researched.

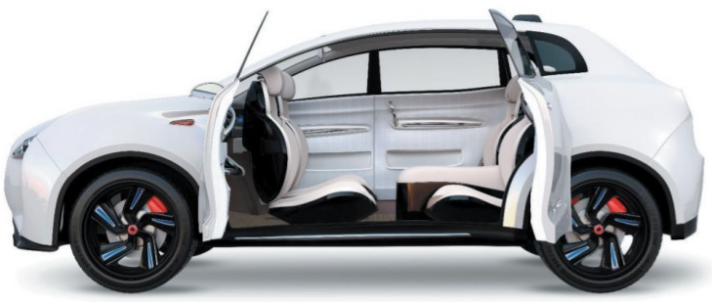

Figure 1.2: SAE level 4 concept car interior design [9]. Here drivers might not even face forward.

1.2.2. Safety

Generally, a driver does not have much experience with unstable behaviour of a vehicle [33]. As a result the driver is often unable to regain control of the vehicle during such event. To aid the driver and to increase safety, an autonomous system that takes control of the drifting motion would be beneficial, as it would be able to guide the vehicle into a safe trajectory. This is why autonomous drift control is introduced as an addition to current ADAS, as it can increase traffic and vehicle safety.

Looking at empirical evidence, expert rally driving techniques, such as driver controlled drifting, could suggest that they can be beneficial for exploiting the full chassis potential on extreme road surfaces. On these surfaces, the tyre cornering stiffness is greatly reduced and sufficient lateral friction levels can only be built up by large body sideslip angles [26]. This leads to the conclusion that vehicle safety on loose surfaces can be increased by drifting based strategies during limit lane departure situations. An example of this would be a vehicle that approaches a turn at excessive speed.

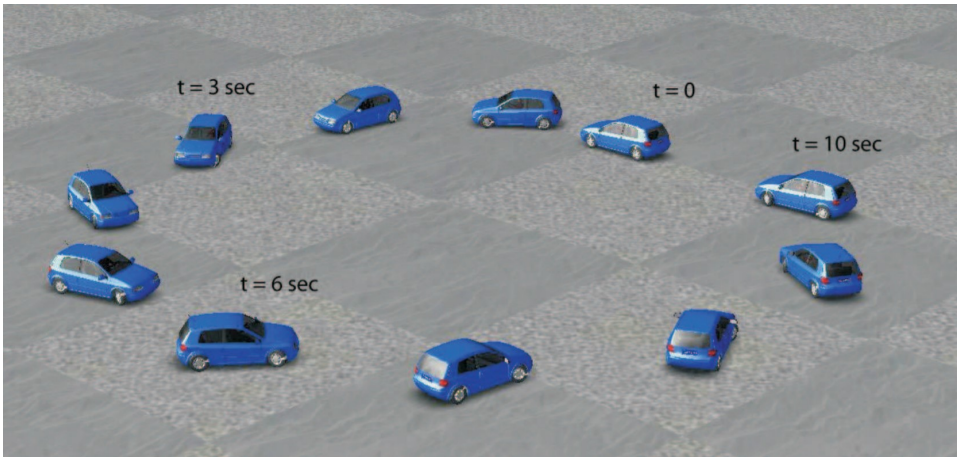

Figure 1.3: Trajectory of a rear-wheel drive vehicle during stabilization [32].

Keeping this in mind, new concepts like autonomous drift control [32] [27] and vehicle agile manoeuvring [29] are considered. The main goal of these researches is to gain a better understanding of the principles of the vehicle dynamics involved in expert drivers driving patterns and especially those in critical conditions. Extensive and broad research of this driving behaviour could result in the development of more sophisticated, safer and even more 'intelligent' chassis systems. In the long term, this can elucidate the path to even more advanced autonomous vehicles which are capable of dealing with any critical situation and drive safely regardless of the road surface, known as full level autonomy [24].

To gain a better understanding of the vehicle dynamics involved in the expert drivers driving patterns of drifting, rear-wheel drive vehicle stabilization for cornering equilibria at aggressive sideslip angles has been studied [32]. In this work a data collection experiment was performed. An expert driver performed a steady state drift on a loose surface (dirt on tarmac) while aiming for a constant speed, sideslip angle and constant radius. During the execution of the drift, sensors fitted to the vehicle collected information on the states of the vehicle. The collected data is shown in Figure 1.4. Analysing the data, it was concluded that drifting stabilization of a rear-wheel drive vehicle, shown in Figure 1.3, requires both steering and throttle regulation. To resemble the experimental drifting motion a simulation was performed in a high fidelity simulation environment. Therefore a vehicle model with non-linear tyre characteristics was first introduced. Using this model the steady state cornering states and inputs were calculated numerically. A realistic drive train model was incorporated as well, such that the input variables of the system were directly correlated to the throttle and steering commands of the driver (in the form of steering angle and rear differential drive torque). A sliding mode controller was then posed for vehicle stabilization at the drifting equilibria. The controller combined drive torque and steering angle inputs, resembling the experimental observations.
In other research a safety system is posed that utilizes rear tyre saturation to mitigate the severity of a T-bone collision (as shown in in Figure 1.5) [8]. This is a collision where vehicles travel in perpendicular directions. The systems that is posed in this research consists of a controller that rapidly re-orientates

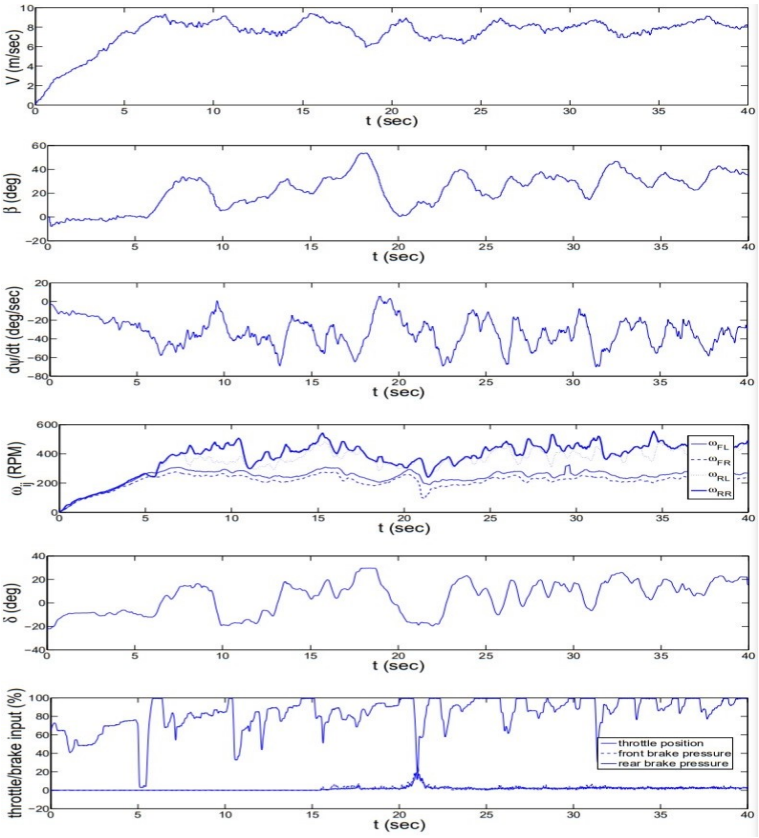

Figure 1.4: Driver input data and vehicle states [32].

Figure 1.5: A T-bone collision [25].

one of the vehicles, such that they become parallel to each other. A decision making map for the system is described as well, stating when either rear tyre saturation should be used or the brakes should be applied. This decision making map is made for three specific cases for rear-wheel driven vehicles, described in Table 1.1.

Table 1.1: The three case descriptions [8].

Case	Initial Speed V_0 [km/h]	Friction Coefficient μ
1	40	0.80
2	55	0.80
3	72	0.80

Next, the option windows for each case were specified, shown in Table 1.2. Furthermore, Table 1.3 describes three zones with their respective recommended actions. These zones, which are also shown in Figure 1.6, show which action should be taken depending on the longitudinal distance between the vehicle and an obstacle. As can be seen from Figure 1.6, there is a zone (Z-1) where the vehicle is

Table 1.2: Option windows for the three cases [8].

Case	Speed [km/h]	Stopping Distance [m]	Rotation Distance [m]	Option Window [m]
1	40	26	15	11
2	55	41	24	17
3	72	60	35	25

Table 1.3: Recommended actions for the three considered cases [8].

Zone	Braking to stop	90 deg. Rotation	Recommended Action
Z-1	Impossible	Impossible	Rotate
Z-2	Impossible	Possible	Rotate
Z-3	Possible	Possible	Brake

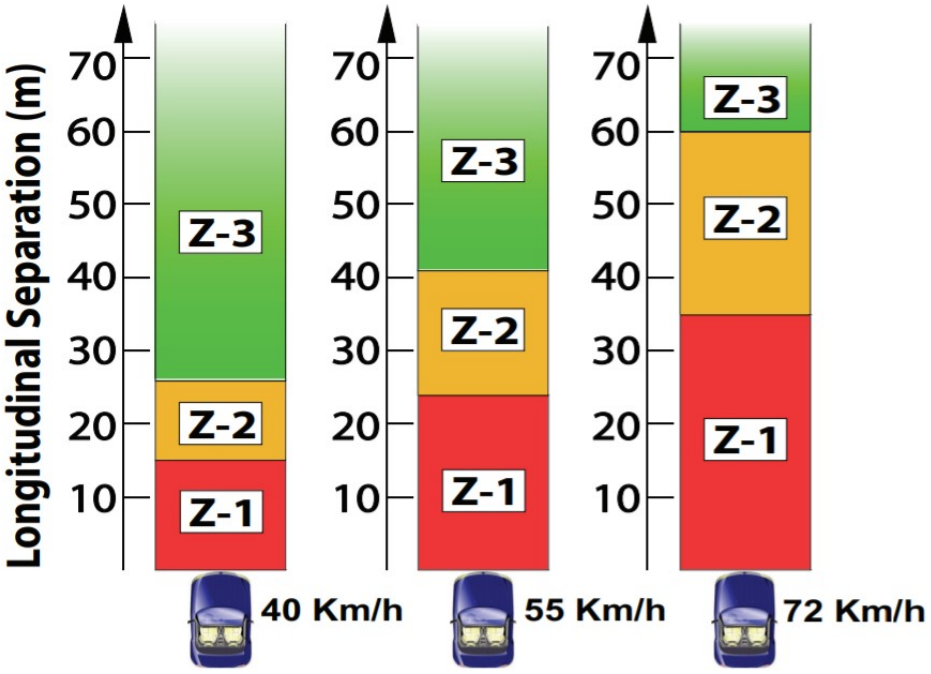

Figure 1.6: Decision making options for different velocities and longitudinal distances between the vehicle and an obstacle. [8].

incapable of stopping by braking or rotating the vehicle towards a safer position. In the second zone (Z-2) the severity of an oncoming crash can be mitigated by rotating the vehicle. In the final zone (Z-3), the vehicle can come to a full stop before reaching the obstacle.

In [15] motion primitives are generated through a four wheel non-linear dynamic model, which form the

basis for a high-level planner. Drifting manoeuvres and parameterized clothoids are utilized to improve vehicle agility. The posed control method is then used to present simulative results. The research also shows experimental results with a ground vehicle on an icy surface, traveling at high speed.
Figures 1.7 and 1.8 show the outcome of the experiments with a passenger vehicle on an icy surface. The path was constructed using parametrized clothoids. The high-level motion primitive path planner was used to test the control framework. Figure 1.7 shows the result of an experiment where the driver was assumed to be distracted. A smoothly planned trajectory could therefore be tracked, as the path tracker assumed control early enough. For the second experiment, shown in Figure 1.8, the controller took over at a later stage. Here the driver was assumed to be attentive. Subsequently the controller only took hold when the planned path became aggressive. To enlarge the feasible region in this situation, braking was invoked. As can be seen in both figures, the obstacle was successfully avoided for both experiments.
Looking at the results of the experiments, it can be concluded that the actual path of the vehicle does not completely correspond to the planned path. According to [15] this was caused by model mismatch, which caused infeasibility of tracking.

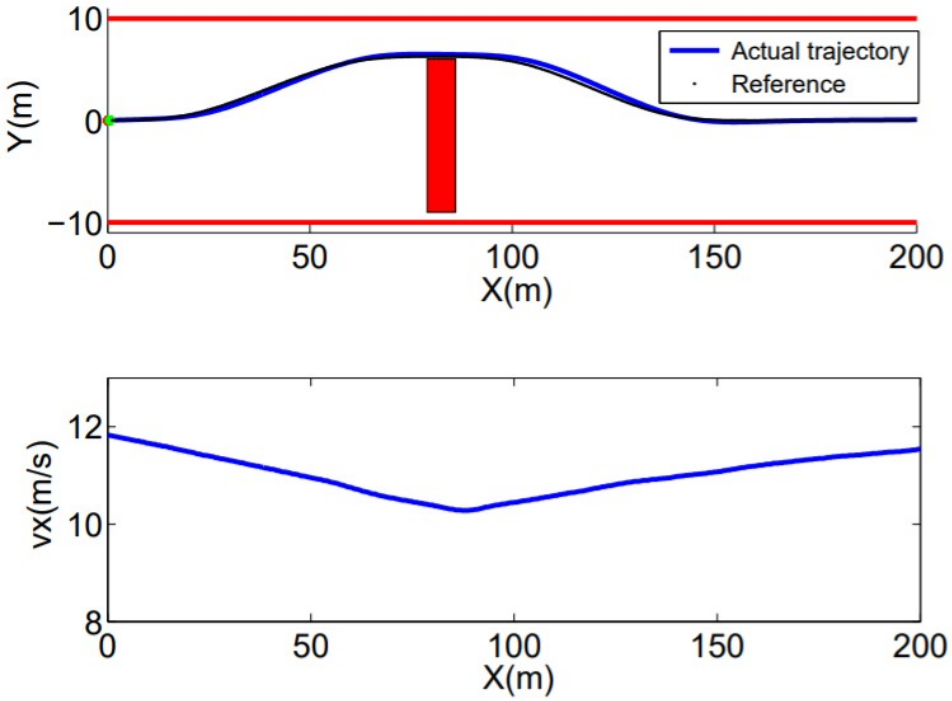

Figure 1.7: The obstacle is successfully avoided by the vehicle using clothoid based manoeuvres. [15].

1.2.3. Performance

In rally sport, drivers use drifting to maximize their cornering speed and therefore minimize their cornering time [26]. In this research minimum time cornering was investigated for various transmission layouts. The layouts that were considered were front-wheel, rear-wheel and all-wheel drive. Nonlinear optimal control techniques were used to create an 'optimal driver' that controlled the vehicle at its handling limits. Simulations were then performed for various road surfaces; dry and wet tarmac, dirt and gravel. It became clear that depending on the transmission layout and the road surface the minimum cornering time was achieved by either typical cornering or drifting. Front-wheel drive vehicles performed better using typical cornering, whereas rear-wheel drive and four-wheel drive vehicles performed better by utilizing a drifting motion.
Next to minimizing cornering time, corner exit velocity can also be a benefit of autonomous drifting [30]. By use of a bicycle vehicle model and numerical optimization a trajectory that maximizes corner exit velocity at a 90° corner was determined. Under normal traction conditions the vehicle behaved as shown in Figure 1.9a. This figure shows the vehicle steering itself to the edge of the lane, maximizing the corner radius. Therefore acceleration can commence at an earlier stage, resulting in a corner exit

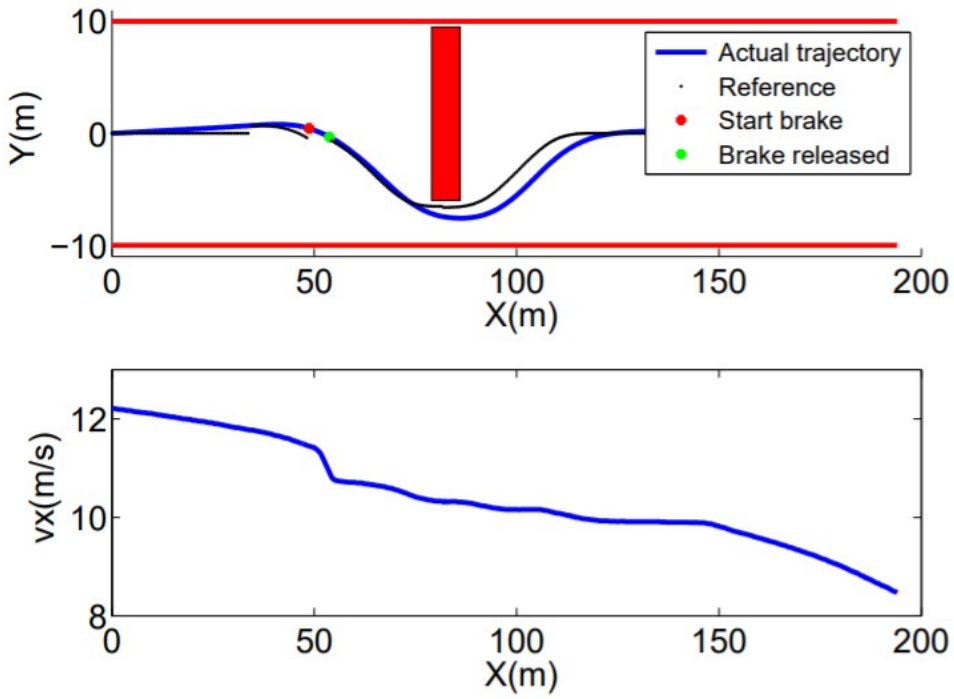

Figure 1.8: Actual trajectory and velocity of the vehicle during the experiment [15].

velocity that was 13% higher than the case where minimum time cornering was considered. The time to travel through the corner did however increase by 37%.

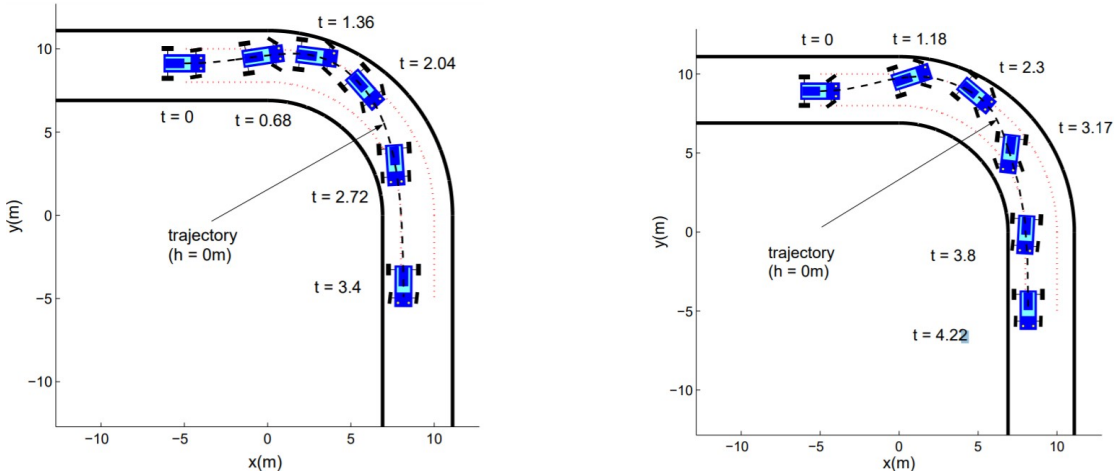

(a) Trajectory for maximum exit velocity.

(b) Drifting trajectory for maximum exit velocity.

Figure 1.9: Vehicle trajectories for maximum exit velocity at different road surfaces [30].

For a neutral-steering vehicle with reduced lateral tyre friction, the highest corner exit velocity was found at large vehicle sideslip angles. This is shown in Figure 1.9b and implies that another performance aspect of autonomous drifting is to maximize cornering exit velocity.
Entering and maintaining a drifting motion is not excluded to four-wheel drive and rear-wheel drive vehicles [28]. For a front-wheel drive vehicle drifting shows two possible benefits. This is done by performing a handbrake cornering technique, where the handbrake is applied to saturate the rear tyres. A front-wheel drive bicycle model configuration with locked rear axle was used to examine the existence of high-sideslip cornering equilibria. This revealed that, for higher values of sideslip angles, higher cornering velocities were achieved while counter-steering on low friction surfaces. Furthermore, the handbrake cornering technique could be used to achieve lower corner radii equilibria when the steering angle was headed towards the direction of the corner. By using this technique, cornering radii could be achieved that were significantly lower than the kinematic turning radius. Additionally, locking the rear axle on a front-wheel drive vehicle can be used to eliminate understeer.

1.3. Problem definition

In order to further progress in the evolution of vehicle safety, more driver assistance systems are developed. Autonomous drifting could become one of those systems. However, as the variety of commercial passenger vehicles and tyre choices is very wide, the effect of the vehicle parameters on the drift equilibria becomes an important aspect.

To progress in the development in safety systems that rely on drift equilibria, general differences between commercial vehicles like mass, geometry and steering characteristics and their effect on drift equilibria points should be investigated. The same goes for the tyre parameters.
Additionally the method that is used to identify drift equilibria should be investigated as well, as due to the unstable nature of drifting a reliable reference point becomes essential.

1.4. Contributions

The investigation on the effect of vehicle parameter variation and tyre model for determining drift equilibria points is the primary contribution of this work. To be able to measure the effects of these aspects, a method is shown on how to determine drift equilibria. Furthermore, the full range of drift equilibria for a curvature of constant radius is elaborated on, for various vehicle parameters and tyre models.

The novelty that is brought forward in this report consist of two parts. First the influence of basic vehicle parameter variation on drift equilibria is investigated. Furthermore, the influence of tyre model selection for the determination of drift equilibria is researched.

1.5. Thesis Layout

This report consists of five chapters. Chapter 1 provides an introduction on drifting. The background of the phenomenon is stated, as is the research relevance and the state of the art.
Chapter 2 describes the full theoretical, including the mathematical, explanation of the three state bicycle model and the considered tyre models. These are the Linear tyre model, Dugoff tyre model and Magic Formula Tyre Model.
In Chapter 3 the method is shown on how to determine drift equilibria and visualize these using a phase plane representation. Furthermore, drift equilibria for different steering characteristics and tyre models are shown and discussed.
In Chapter 4 drift equilibria are set up and discussed for several varying vehicle parameters, including the vehicle geometry, mass and tyre stiffness. Additionally this done for comparison between the Dugoff tyre model and the Magic Formula Tyre Model.
Finally, the research is concluded in Chapter 5. Recommendations for further research are given in this chapter as well.

2

Vehicle Modelling

2.1. Vehicle Model

2.1.1. Bicycle Model

The behavior of a vehicle can be generally described by its dynamic equations. Quantities that can be used to describe the dynamics of the bicycle model are, amongst others, the vehicle mass and dimensions [33]. When seen from above, there are a number of aspects that can be observed regarding the bicycle model negotiating a certain path. Two key characteristics can instantly be identified when

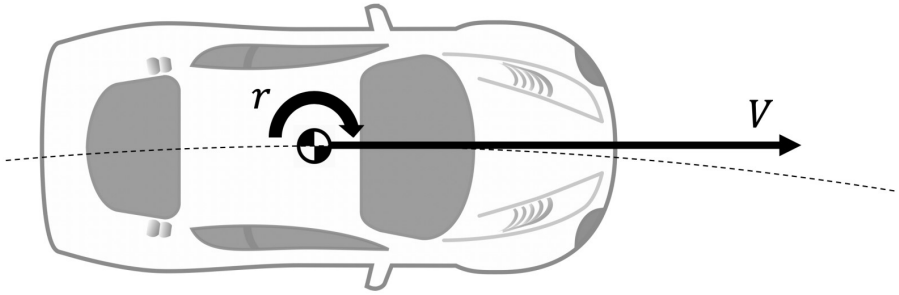

Figure 2.1: A vehicle taking a right hand side corner [33]

analysing the vehicle in Figure 2.1, which is driving along the dashed path. The vehicle is driving at a certain velocity (V). Furthermore, the vehicle can negotiate a curved trajectory (κ_t) through a slight rotation around its Center of Gravity (CoG). The characteristic behavior of this vehicle can generally be described by two equations. The curvature which the vehicle is traveling and the overall velocity of the vehicle are described by these equations.

$$\kappa_t = \frac{r}{V} \tag{2.1}$$

$$V = \sqrt{v_x^2 + v_x^2} \tag{2.2}$$

Where the longitudinal velocity, the lateral velocity and the yaw rate are described by v_x, v_y and r respectively. Using differential equations to describe vehicle dynamics, these three quantities form the first physical states. Dynamical modeling of vehicle behavior can happen through various ways, accounting for or omitting specific characteristics and if possible by simplifying the system. Vehicle dynamics can be captured by more extensive or simple models. In extensive models a full-car model includes for example roll, pitch and yaw dynamics, modeling for sprung and unsprung masses to show the behavior of the suspension system and external forces such as air resistance. Such complex models can be simplified into a two track model, which exists of a rigid body and four wheels, and even

further simplification is an option.

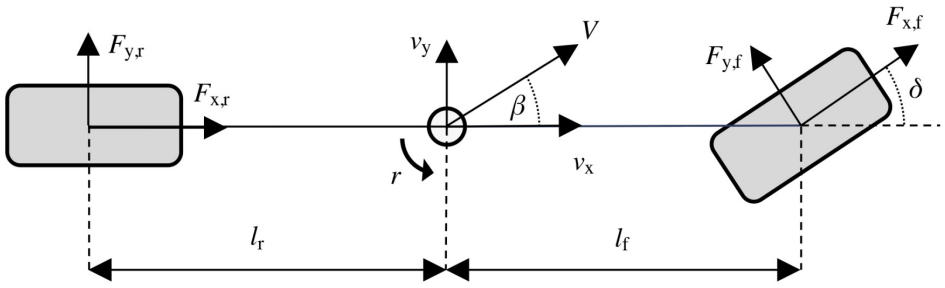

Figure 2.2: Bicycle model [33].

To simulate the vehicle dynamics, the three-state bicycle model is used. This model is described by a diagram, which can be seen in Figure 2.2. When the two front wheels and two rear wheels are fused together into one front wheel and rear wheel, the vehicle dynamics can be simplified. Steering the front wheel results in a change of the direction in which the vehicle is heading (right in Figure 2.2). The steering angle (δ) describes the angle of the front wheel.

The vehicle mass is modeled at a single point, at the centre of gravity of the vehicle, which separates the front and rear of the vehicle. This simplification is based on an elimination of the pitch and roll dynamics and the assumption that the vehicle consists of a rigid body. According to the Newton-Euler balances, the accelerations and rotation of the vehicle are determined by forces acting on the tyres. This behavior is described by the following differential equations:

$$\dot{v}_x = \frac{1}{m}(F_{x,r} + F_{x,f}\cos(\delta) - F_{y,f}\sin(\delta)) + v_y r \tag{2.3}$$

$$\dot{v}_y = \frac{1}{m}(F_{y,r} + F_{x,f}\sin(\delta) + F_{y,f}\cos(\delta)) - v_x r \tag{2.4}$$

$$\dot{r} = \frac{1}{I_z}(F_{x,f}\sin(\delta)l_f + F_{y,f}\cos(\delta)l_f - F_{y,r}l_r) \tag{2.5}$$

Where m, F and I_z describe the vehicle mass, the forces acting on the tyres and the vehicle yaw inertia respectively. The distance from an axle to the centre of gravity is described by l. The superscripts x and y respectively describe the longitudinal and lateral direction, whereas f and r represent the front and rear axle.

2.2. Tyre Model

The forces, generated at the tyres, influence the velocity and behaviour of the vehicle. At this point, there is an interaction between the road and the tyres. Forces acting on the tyres occur due to friction, generated by the relative velocities of these two materials. Various properties of both the tyres and the road, along with the normal forces from the vehicle acting on the tyres, determine the magnitude of the force. Furthermore the type of road surface needs to be taken into consideration, as there are multiple types which leads to various interactions between the road and the tyre [33]. The road friction coefficient (μ) is used in order to describe how much of the vehicles normal force acting on the tyres can maximally be translated into friction, which in turn generates forces on the tyres. A road friction coefficient of approximately $\mu = 1$ is ,for example, typical for a dry asphalt road, whereas a road friction coefficient of $\mu = 0.1$ matches an icy surface.

Multiple models have been developed to show this interaction between the road and tyres and to determine the forces which are acting on the tyres [11] [14]. Pros and cons apply to each model about whether the formulation is based on physical characteristics or empirical design. This also applies on the consideration if the complexity and accuracy fit the rate at which the forces are to be quantified.

2.2.1. Linear Tyre Model

The linear tyre model is a relatively simple model with low computational costs. The forces acting on the tyres are given by the following equations:

$$F_x = C_x \kappa \tag{2.6}$$

$$F_y = C_y \alpha \tag{2.7}$$

Here the forces F acting on the tyres are calculated by multiplying the longitudinal and lateral slip ($/kappa$ and $/alpha$) with their respective tyre stiffnesses C. A drawback of this method is that it assumes that the tyre is always acting within its linear dynamic behaviour. As drifting behaviour happens in the non-linear region of tyre behaviour, this method can not be used to determine drift equilibria.

2.2.2. Dugoff Tyre Model

As opposed to the linear tyre model, combined longitudinal/lateral slip tyre forces can be determined using the Dugoff tyre model [11]. Here the longitudinal and lateral tyre friction forces are described by relatively simple equations and an if-statement. As a result of the relatively simple equations, the computation costs are low [6]. The most important advantage of the Dugoff tyre model is that it includes the maximum road friction coefficient μ_0, adopting the estimation of road friction potentials and road conditions. The utility of this tyre model is however limited, due to being incapable of determining the tyre force dynamic characteristics with the change of wheel slip.

By utilizing the Dugoff non-linear tyre model, the forces on both the front and rear axles can be calculated using the following equations [11]:

$$F_x = \frac{C_x \kappa}{1 - \kappa} f(\lambda) \tag{2.8}$$

$$F_y = \frac{C_y \tan(\alpha)}{1 - \kappa} f(\lambda) \tag{2.9}$$

where $f(\lambda)$ is a weighting function, defined as:

$$f(\lambda) = \begin{cases} \lambda(2 - \lambda), & \text{if } \lambda < 1 \\ 1, & \text{if } \lambda > 1 \end{cases} \tag{2.10}$$

The weighting coefficient λ is given by the equation:

$$\lambda = \frac{\mu F_z (1 - \kappa)}{2\sqrt{(C_x \kappa)^2 + (C_y \tan(\alpha))^2}} \tag{2.11}$$

Where the friction coefficient μ and normal force F_z are given by:

$$\mu = \mu_0 (1 - e_r V_x \sqrt{\kappa^2 + \tan^2(\alpha)}) \tag{2.12}$$

$$F_z = \frac{mgl}{L} \tag{2.13}$$

Where L is the wheelbase, defined by $l_f + l_r$. The friction reduction coefficient and the gravitational acceleration are respectively described by e_r and g.

2.2.3. Pacejka Tyre Model (Magic Formula)

The Magic Formula, given by Equation 2.14, can be used to quantify the longitudinal and lateral forces acting on the front and rear tyres. Due to low computational costs in combination with accurate achievements when enough empirical data is used, it is possible to use this semi-empirical model for design purposes [4]. Low computational costs are beneficial for high-frequency computation, while the sin(arctan) formula is ideal for F_x and F_y curves. This is shown in Figure 2.3. For vehicle dynamics control these properties are critical elements. The complete Magic Formula tyre model is composed of more than twenty formulas, using over 100 parameters to calculate longitudinal and lateral forces and self-aligning

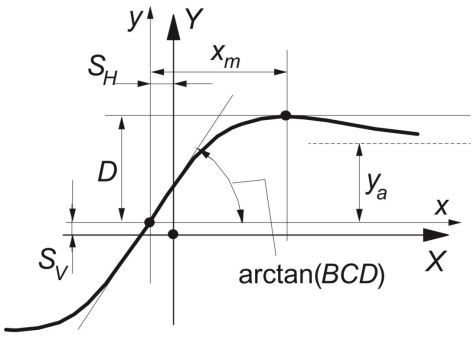

Figure 2.3: $X - Y$ curve produced by the original Magic Formula [21].

moments acting on the tyres. However, this does not benefit high-rate computations. Therefore a simplified model, proven successfully in the area of autonomous drift control, is used [1].

$$y(x) = D\sin(C\tan^{-1}(Bx - E(Bx - \tan^{-1}(Bx)))) \tag{2.14a}$$

with

$$Y(X) = y(x) + S_v \tag{2.14b}$$

$$x = X + S_h \tag{2.14c}$$

X and Y are the respective input and output variables in the Magic Formula. In the simplified formulation, there are six variables, namely the stiffness factor (B), the shape factor (C), the peak value (D), the curvature factor (E), the horizontal shift (S_h) and the vertical shift (S_v). In the Magic Formula, the variables can be chosen directional dependent for lateral forces and longitudinal forces. Isotropic behavior is assumed. In this research the Magic Formula is formulated as described in [26] to calculate the slip coefficient μ, described by:

$$\mu = \frac{\sigma_i}{\sigma} D\sin(C\text{atan}(\sigma B - E(\sigma B - \text{atan}(\sigma B)))) \tag{2.15}$$

$$F = \mu F_z \tag{2.16}$$

Where the i in σ_i indicates the lateral or longitudinal theoretical slip quantity. Here, the theoretical slip quantities (Equations 2.21 - 2.23) are used to form a coupling between longitudinal forces and lateral forces [21]. In this formulation, the horizontal and vertical shift of the friction curve is neglected.

2.2.4. Wheel dynamics

If a relative motion between two surfaces exist, slip occurs. Putting this in to perspective of tyre-road interaction, this relative motion arises between the contact area of the tyre, which is traveling due to the wheel angular velocity [33], and the velocity at which the overall vehicle is moving with respect to the road surface. It is assumed here that the tyres are perfectly round and that the vehicle consists of a rigid body. The wheel rotational velocity ω can be expressed in terms of the longitudinal velocity v_x and the wheel radius r_ω. Furthermore, torque T_{net} can be applied to the wheels, which will influence the angular wheel acceleration $\dot{\omega}$. The mathematical descriptions of these behaviours are given by:

$$\omega = \frac{v_x}{r_\omega} \tag{2.17}$$

$$\dot{\omega} = \frac{1}{I_\omega}(-F_x r_\omega + T_{net}) \tag{2.18}$$

Where I_ω describes the wheel inertia. The difference in relative motion of the tyre surfaces and the vehicle can be commonly described by the longitudinal wheel slip coefficient κ:

$$\kappa = \frac{r_\omega \omega - v_x}{\max(r_\omega \omega, v_x)} \tag{2.19}$$

The front and rear lateral wheel slip angles α_f and α_r are determined as follows:

$$\begin{bmatrix}\alpha_f \\ \alpha_r\end{bmatrix} = \begin{bmatrix}-\beta + \delta - \frac{l_f r}{u} \\ -\beta + \frac{l_r r}{u}\end{bmatrix} \tag{2.20}$$

With sideslip angle β, steering angle δ, vehicle velocity u, yaw rate r and respective front and rear axle to CoG distances l_f and l_r. The forces acting on the vehicle can then be determined by utilizing one of the tyre models described above.

In order for the Magic Formula Tyre Model to be able to account for combined slip situations, theoretical slip quantities are set up as shown in Equations 2.21 - 2.23. Once calculated, these theoretical slip quantities can then be used in the deviation of the Magic Formula as described in [26].

$$\sigma_x = \frac{\kappa}{\alpha + \kappa} \tag{2.21}$$

$$\sigma_y = \frac{\tan(\alpha)}{1 + \kappa} \tag{2.22}$$

$$\sigma = \sqrt{\sigma_x^2 + \sigma_y^2} \tag{2.23}$$

In this work, net rear wheel torque T_{net} and steering angle δ are applied in order to find drift equilibria.

2.3. Tyre forces

To better understand the three tyre models, which are mathematically explained in the previous sections, the tyre forces resulting from each respective tyre model can be considered [22].
In order to construct a proper comparison using the tyre forces, the tyre stiffnesses that are used have to be equal for every tyre model. This initially poses a problem as the Magic Formula Model utilizes four tyre parameters (B, C, D and E) in stead of the three tyre stiffnesses (C_κ, $C_{\alpha f}$ and $C_{\alpha r}$) used in the Linear Tyre Model and Dugoff Tyre model. This problem can however be overcome as the Magic Formula Model tyre parameters can be converted into tyre stiffnesses using:

$$\begin{bmatrix}C_{\alpha f} \\ C_{\alpha r}\end{bmatrix} = \begin{bmatrix}B * C * D * F_{z,f} \\ B * C * D * F_{z,r}\end{bmatrix} \tag{2.24}$$

Where the tyre parameters B, C, D and E are stated in Table A.2. The longitudinal slip stiffness is chosen to be $C_\kappa = 1.2 * C_\alpha$.
Now the tyre force graphs can be constructed. This is done by considering each axle individually and only accounting for lateral slip α and longitudinal slip κ for lateral forces F_y and longitudinal forces F_x respectively. In other words, pure longitudinal slip ($\alpha = 0$ rad) is considered for calculation of the longitudinal tyre forces, whereas pure lateral slip ($\kappa = 0$) is considered for calculation of the lateral tyre forces. Figure 2.4 shows the outcome of these calculations. As can be seen from Figure 2.4, all three tyre models show different behaviour outside the linear range of the tyre. The linear tyre model shows, as its name suggests, a linear behaviour over the full range of lateral and longitudinal slip. The Dugoff tyre model shows a decrease in both lateral and longitudinal force gain with a respective increase in lateral slip angle and longitudinal slip. The Magic Formula model shows similar behaviour as the Dugoff tyre model with its decrease in both lateral and longitudinal force gain. The big difference between the two latter tyre model is that the Magic Formula model shows a clear peak in lateral force F_y and longitudinal force F_x at $\alpha \approx 0.14$ rad and $\kappa \approx 0.16$ for both the front and rear axle. The peak lateral and longitudinal force for the Dugoff tyre model is reached at larger respective lateral slip angles α and longitudinal slip κ. Using the Dugoff tyre model, the peak lateral force is achieved at lateral slip angle $\alpha \approx 0.35$ rad. The peak longitudinal force is reached at longitudinal slip $\kappa \approx 0.3$.
Taking these tyre model characteristics into account, the determined drift equilibria using these models is shown in the following section. Again the vehicle parameters stated in Table A.1 are used, resulting in a vehicle with neutral steering characteristics $K_{us} = 0$. Additionally, for the Magic Formula Model the tyre parameters shown in Table A.2 are used.

Furthermore, the graphs shown in Figure 2.4 are used to tune the Dugoff tyre model. Tuning this tyre

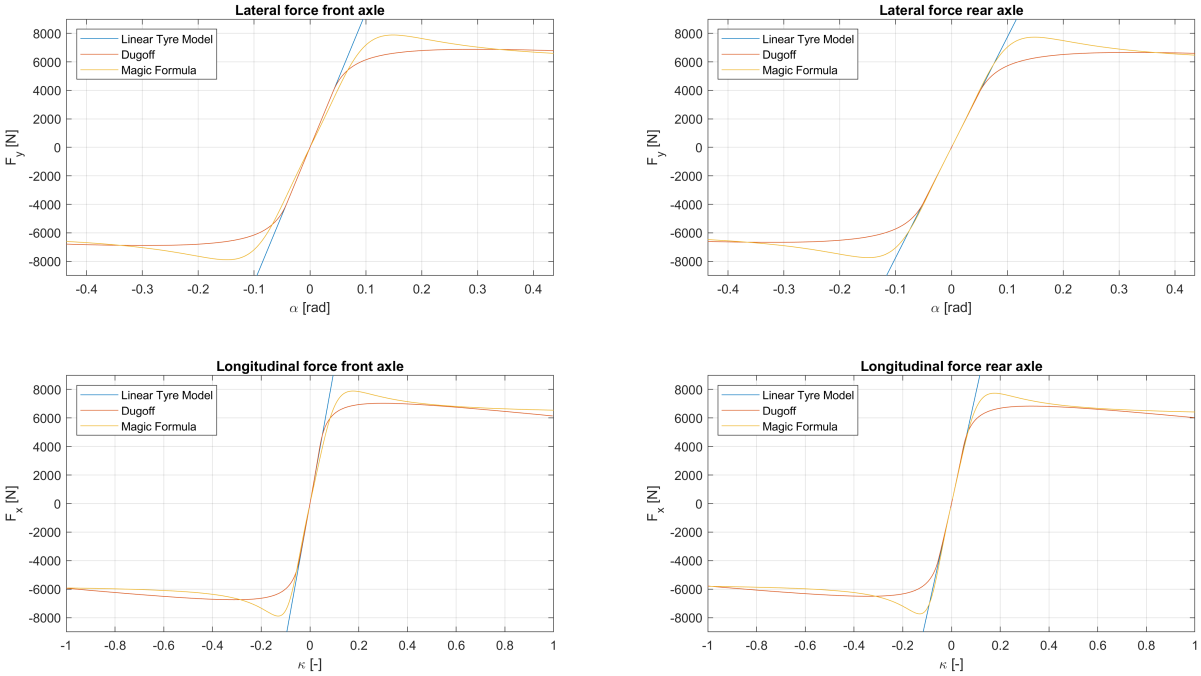

Figure 2.4: Tyre forces for the Linear Tyre Model, Dugoff Tyre Model and Magic Formula Model.

model can be done by adjusting the peak friction coefficient μ_0 and the friction reduction coefficient e_r. These values were adjusted such that the resulting tyre force diagram of the Dugoff tyre model resembles the tyre force diagram of the Magic Formula model as close as possible. The purpose of this tuning is to be able to compare these two tyre models more accurately.

2.4. Summary

Chapter two shows all the main mathematical parts and their descriptions that are necessary in order to eventually discover drift equilibria. In this research the vehicle model is chosen to be the three state bicycle model, which is mathematically described using differential equations.
Next, the tyre models are elaborated on. First the linear tyre model, which assumes the linear region of tyre is infinite, is briefly introduced. Secondly the Dugoff tyre model is both generally and mathematically explained. This tyre model does in fact account for non-linearities in tyre behaviour. The final tyre model that is shown has this feature as well, which is the Magic Formula Tyre Model. In order to do so, wheel dynamics and theoretical slip quantities were introduced.
Finally, the tyre forces resulting from the stated tyre models are shown and discussed.

3

Stability analysis

3.1. Phase Plane

3.1.1. High sideslip manoeuvring

Vehicle motion can become of a less constraint form by adding rear tyre saturation cornering to typical vehicle cornering. This is mainly caused by the fact that during cornering with rear tyre saturation the heading of the vehicle and the direction of its centre of gravity (CoG) are decoupled, whereas these two terms are coupled during typical cornering [17].

Comparing the vehicle motion during drifting and typical cornering in vehicle dynamics terms helps to understand why this is true. Looking at the local coordinate system of a vehicle centered at its CoG, the following terms in the (x, y)-plane describe the motion of the vehicle; velocity vector V at the CoG, sideslip angle β (between the velocity vector and the x-axis of local coordinate system), and angular velocity r (about the z-axis of the local coordinate system).

To understand the motion of the vehicle it is also important to know the velocity vectors at the locations of the tyre contact patches with the road surface as these quantities greatly influence the way in which the dynamics of the vehicle are modeled. The velocity vectors at the contact patches and the velocity vector at the CoG are related via kinematic equations [17]. As a result the velocity vectors at the contact patches can be used to determine the velocity vector at the CoG and the vehicle yaw rate, and vice versa.

However, models based on force constraints, rather than on kinematic constraints, capture the dynamic behaviour of a vehicle better [17]. These models are dictated by generated lateral tyre forces through tread deflection in the contact patch. The lateral forces result from a non-zero wheel slip angle α at the tyres. Similar to the vehicle sideslip angle β, the wheel slip angle α represents the angle between the velocity vector at the contact patch and the direction that the tyre is pointing. Through steering the slip angles, and therefore the lateral forces, can be adjusted at the front tyres. The slip angles at the rear tyres evolve with vehicle motion. Force constraint based models treat the vehicle as a holonomic system subject to friction limitations due to tyre properties [17]. As a result the system is subject to force constraints. The amount of force acting on the tyre of a vehicle rises with rising wheel slip angle, but this is not unlimited. At some threshold value for α, the available friction can no longer support tread deflection in the contact patch. In case of this event the tyre saturates.

At slip angles of about 0.07 rad tyre force saturation typically occurs. This means that within a relatively small slip angle the entire spectrum of typical cornering is encompassed, from everyday driving to racing [17]. Following the small tyre slip angles during cornering, β remains small as well. This is visualized in the left half of Figure 3.1. As a result, when modeling typical cornering , the heading of the vehicle and its velocity vector at the CoG are tightly coupled.

When observing a drifting motion, it is clear that tyre saturation is an inherent aspect. Therefore the small slip angle restrictions for the rear tyres, which are normally present at typical cornering, must be denied. During a drift, the tyre slip angles can reach tens of degrees [17]. Following the kinematic relationships this results in a large vehicle sideslip angle β that typically characterizes a drifting motion.

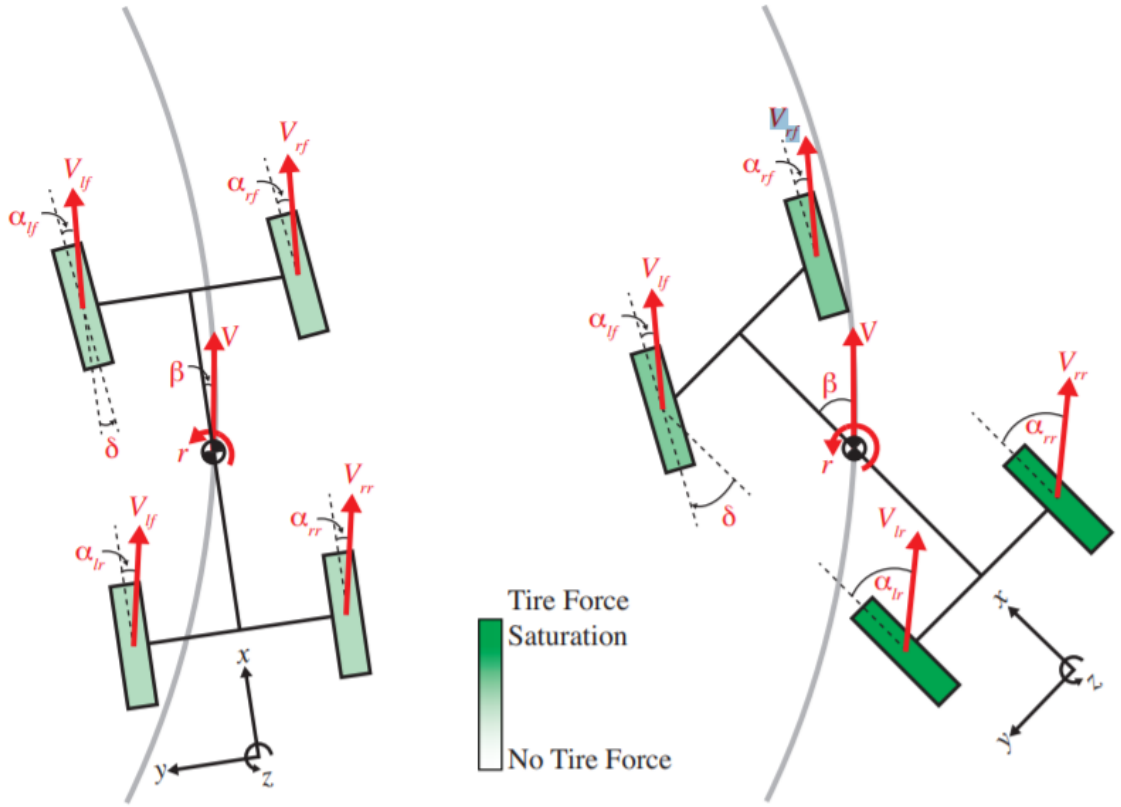

Figure 3.1: Visualization of typical cornering (left) and drift (right) vehicle motion [17].

This is visualized in the right half of Figure 3.1. From this part of the figure it can be concluded that the rear tyre slip angles are no longer constrained. Following the kinematic relationships the vehicle sideslip angle is also no longer constrained. As a result the direction in which the CoG is moving is effectively decoupled from the heading of the vehicle.

On surfaces with uncertain friction, like in rally racing, valuable flexibility to alter the trajectory of the vehicle is gained thanks to this decoupling. Additionally, this phenomenon might improve overall vehicle safety as well [15] [8].

Drifting is defined as a steady state operation with rear tyre saturation. This implies that drifting can be modeled as a vehicle state equilibrium with rear tyre saturation. Current literature confirms this implication as it has been demonstrated repeatedly across a broad range of model fidelities that so called drift equilibria exist [17]. Simple two-state models for the lateral dynamics of a vehicle are used to show the existence of open-loop unstable drift equilibria [5] [7]. These researches employ the phase portrait analysis technique to visualize vehicle trajectories in a sideslip versus yaw rate plane for a fixed vehicle velocity and fixed steering angle. Figure 3.2 shows an example of such a phase portrait. In this figure, three red dots are visible, each representing an equilibrium condition. The two outermost red dots correspond to high-sideslip unstable drift equilibria. The middle equilibrium conditions corresponds to typical cornering. A factor that has to be accounted for is that analysis using lateral dynamics models alone only results in a partial drift equilibria characterization. Drive torques play a critical role in a drift as drift equilibria are associated with large rear wheel torques [12] [29] [31]. Considering the tyre models used in these researches, it becomes clear that a tyre saturates when the total force demand, consisting of a combination of the lateral and longitudinal force, exceeds the available tyre friction force. From this it can be concluded that it is essential to have large rear wheel torques available to reach rear tyre saturation and by that reach drift equilibria. The large rear wheel torques result in large longitudinal tyre forces. This results in rear tyre saturation as the combined lateral and longitudinal forces exceed the friction limits of the tyres.

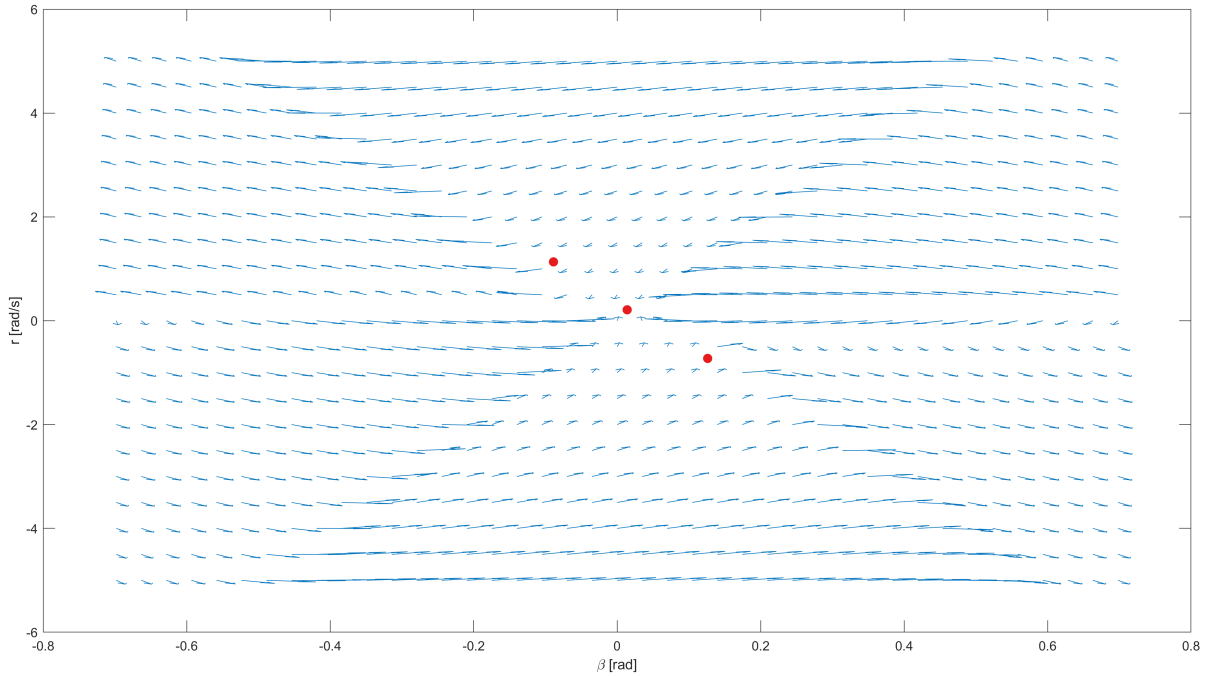

Figure 3.2: Example of a phase plane representation. Three equilibria, depicted by red dots, are visible. The middle equilibrium is stable and corresponds to conventional cornering. The other two are unstable high-sideslip equilibria.

In [12], [29] and [31] vehicle models are used that include longitudinal dynamics in order to incorporate rear drive inputs into the analysis. More elaborate models with five states were used to be able to include longitudinal vehicle dynamics. Additionally to this method, load transfer effects were included as well as more complex tyre models that include longitudinal wheel slip. However, the consequence of using more complex vehicle models was that relatively simple drift equilibria analysis techniques like phase portraits could not be used. Nevertheless, in [12] a root locus analysis was performed to show that drift equilibria are unstable. The root locus analysis of drift equilibrium stability was performed with variations in longitudinal velocity.

Literature thus shows that drift equilibria are unstable, irregardless of the model used for analysis. This conclusion implies that the drifting motion of a vehicle requires closed-loop stabilization of the drift equilibria by a controller.

For this research, steady state equations were set up and solved, after which these were visualized using phase plane representations. The method on how to set up and solve these equations, is shown in the following section.

3.1.2. Steady state solution

To find drift equilibria, the steady state dynamic equations can be solved, as was done to create Figure 3.2. Therefore, first a set of initial conditions will have to be specified. These initial conditions are the vehicle sideslip angle β and yaw rate r. The values that are chosen for β and r are:

$$\beta = -0.6981 : 0.6981 \text{ rad/s } (-40 : 40 \text{ }^\circ)$$
$$r = -5 : 5 \text{ rad/s}$$

These values for the vehicle sideslip angle and yaw rate were chosen based on the values used in [17]. These values where then expanded to create a build-in certainty for drift equilibrium points to became visible if they should exist, resulting in the initial condition ranges shown above. The vehicle velocity $V = u$ and steering angle δ are chosen as 22.22 m/s (80 km/h) and 0.0349 rad (2°) respectively, based on the values used in [22]. The initial conditions for β and r are set up in a grid, as shown in Figure 3.3.

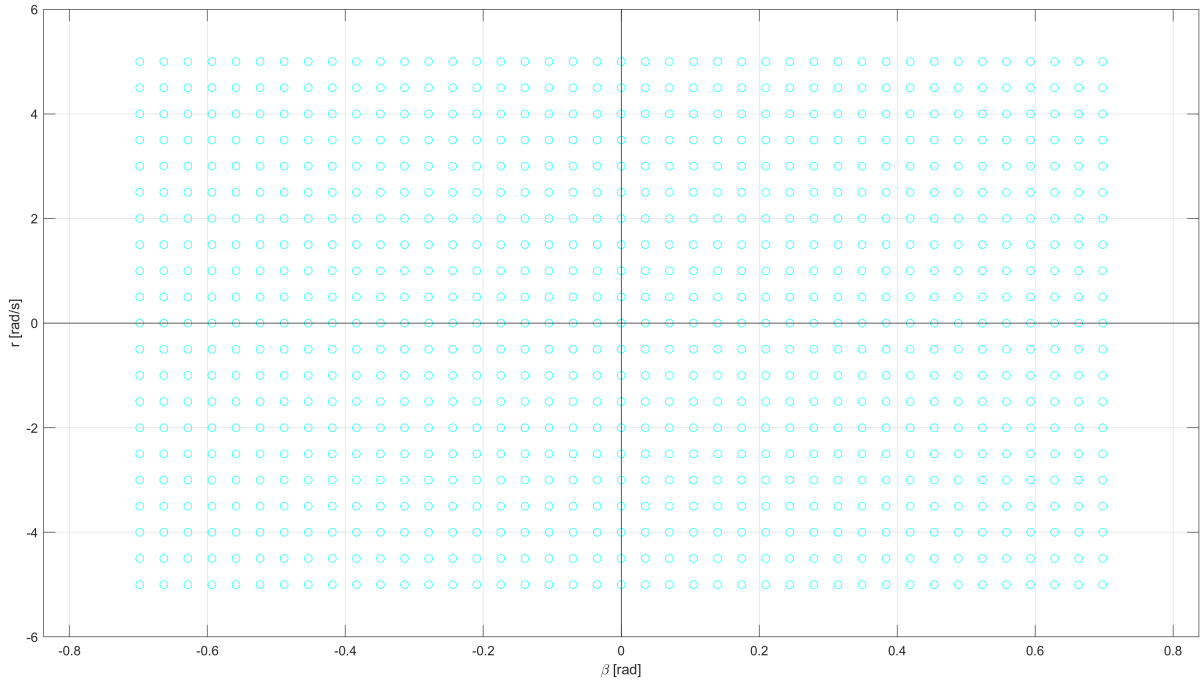

Figure 3.3: Grid of initial conditions for vehicle sideslip angle β and yaw rate r.

From this grid the phase plane diagram can eventually be determined. In this section, the Dugoff tyre model from Section 2.2.2 has been used.

By using the initial conditions and the lateral forces acting on the vehicle F_y, the lateral acceleration a_y can be calculated. Furthermore, the yaw moment M_z can be determined by using normal force F_z, making it possible to calculate the yaw acceleration $\dot{r}$ of the vehicle. The sideslip angle rate $\dot{\beta}$ can then be derived by using the lateral acceleration of the vehicle.

$$a_y = \frac{F_y}{m} - ur \tag{3.1}$$

$$M_z = F_{y,f} l_f - F_{y,r} l_r \tag{3.2}$$

$$\dot{r} = \frac{M_z}{I_z} \tag{3.3}$$

$$\dot{\beta} = \frac{a_y}{u} \tag{3.4}$$

By utilizing the `quiver` command in Matlab, a phase plane representation can be visualized, as will be shown in the next section.

3.2. Different steering characteristics

A vehicle is subject to one of three certain steering characteristics; understeer, neutral steer or oversteer [22]. The relationship described in Equation 3.6 clearly expresses the influence of certain vehicle characteristics on vehicle cornering performance.
At low vehicle velocities, the steering angle that is needed to negotiate a curve is the equivalent of the relative curvature $\frac{L}{R}$ (Ackermann angle). When the vehicle velocity over the same curve (a circle with radius R) increases , a necessary change is created in the required steering angle that is dependent on the understeer gradient K_{us}, and thus on the characteristics of the tyre. The steering angle δ has to increase for a positive understeer gradient K_{us}. Vice versa, for a negative K_{us}, the steering angle δ must be reduced. If the steering angle δ would not be reduced with negative K_{us} and the driver does not take action either, the result is a smaller curve radius, which would further increase the lateral acceleration. This means that there is a self-reinforcing effect within the vehicle, with negative consequences for understeer gradient $K_{us} < 0$, eventually leading to vehicle instability.

Figure 3.4 show the consequences of the three types of steering behaviour and the necessary steering correction with increasing vehicle velocity in a corner with radius $R = 30$ m.

$$\delta = \frac{L}{R} + K_{us}\frac{a_y}{g} \tag{3.5}$$

$$K_{us} = \frac{mg}{L}\left(\frac{l_r}{C_{\alpha,f}} - \frac{l_f}{C_{\alpha,r}}\right) \tag{3.6}$$

Equations 3.5 and 3.6 lead to the following definitions [22]:

1. If the axle steering angle has to be increased for a vehicle while negotiate a curve, the vehicle is understeered. Vice versa, when the steering angle has to be decreased for a vehicle while negotiate a curve, the vehicle is oversteered. If no adjustment of the steering angle has to be made, the vehicle is neutrally steered.

2. If the front axle slip angle exceeds the rear axle slip angle under steady-state conditions ($\alpha_f > \alpha_r$), the vehicle is understeered. Vice versa, when $\alpha_f < \alpha_r$ the vehicle is oversteered.

3. If the understeer gradient $K_{us} > 0$, the vehicle is understeered. This is thus the case when the front axle normalized axle cornering stiffness is exceeded by the rear axle normalized axle cornering stiffness.

4. If the steering wheel gradient $\frac{\partial \delta}{\partial a_y}$ $(a_y = 0)$ is positive, the vehicle is understeered. If the steering wheel gradient is negative, the vehicle is oversteered.

In conclusion, the four definitions are identical for linear tyre characteristics. For larger lateral accelerations where nonlinear axle behavior is not to be neglected, definition 1 applies. definitions 2, 3 and 4 need to be taken into consideration for tyre behavior at small lateral accelerations. In the following section the influence of the three steering characteristics on finding the drift equilibria, using the steady state solution, is discussed. The base tyre stiffnesses, resulting in neutral steering behaviour, are shown in Table A.1. In every case the Dugoff tyre model was used.

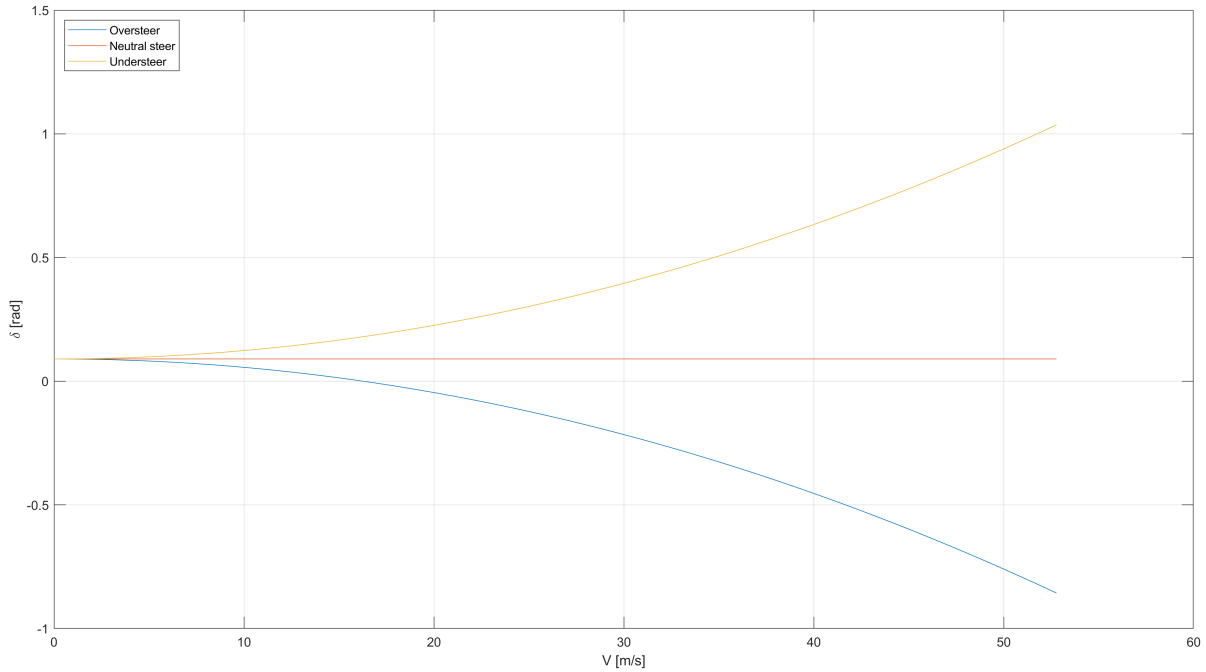

Figure 3.4: Visualization of oversteer, neutral steer and understeer vehicle steering characteristics with increasing vehicle velocity on a curvature of $R = 30$m.

3.2.1. Understeer

As mentioned before and shown in Figure 3.4, a vehicle with understeer steering characteristics should increase its steering angle δ with increasing velocity on a curvature in order to stay on the predetermined path.
In this case the rear axle stiffness was increased by 30% in order to give the vehicle understeer characteristics. The result of this steady state solution, performed like explained in Section 3.1.2, is visualized

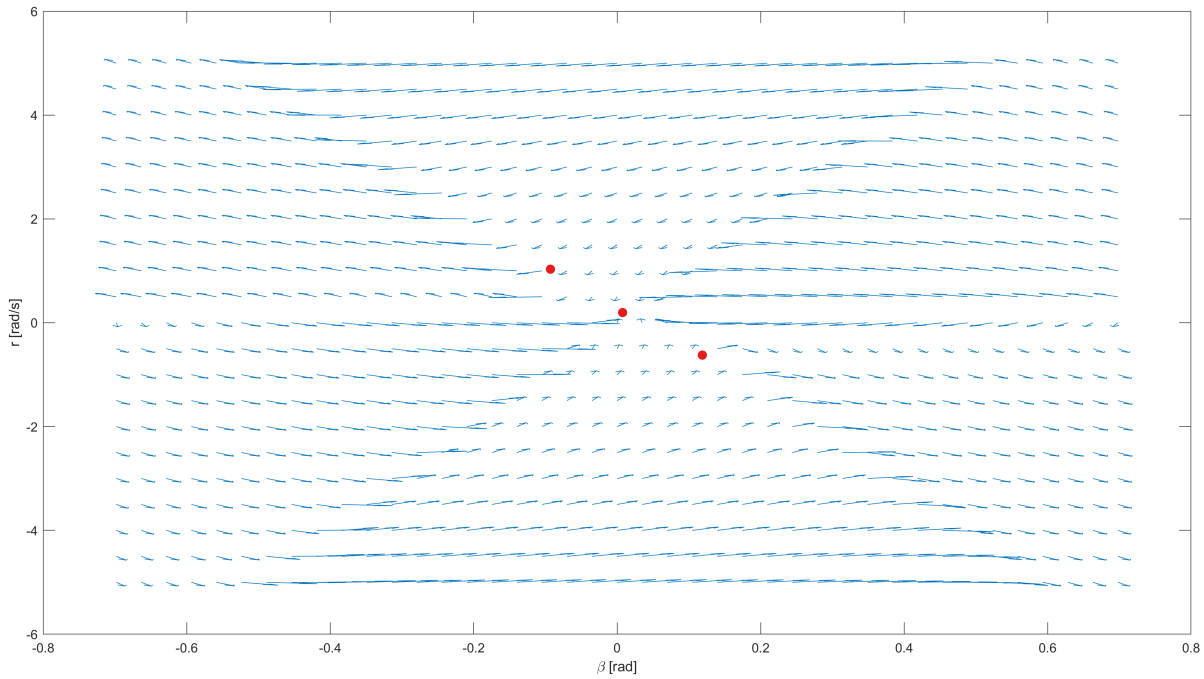

Figure 3.5: Steady state solution for drift equilibria, using Dugoff tyre model and understeering characteristics, visualized in a phase plane diagram.

in Figure 3.5. Following the explanation from Section 3.1.1, three equilibria can be distinguished, shown for clarity reasons by red dots. The locations of the red markings in this figure and following figures were achieved by visual inspection of each individual phase plane diagram. One equilibrium at the centre of the phase plane visualization represents typical cornering. The presence of the other two, unstable, equilibria prove the presence of drift equilibria. Therefore drifting equilibria do exist for an understeering vehicle parameterized by Table A.1.
The arrows visualized in Figure 3.5 and following phase plane diagrams indicate if a vehicle can return to a stable handling situation for initial β and r. If an arrow eventually points towards the centre of the graph, the vehicle can return to a stable handling situation. If an arrow does not eventually point toward the center of the graph, the vehicle is unstable for that β and r combination and spins out of control.

3.2.2. Neutral Steer

A vehicle with neutral steering behaviour does not have to adjust the steering angle δ while negotiating a corner with increasing vehicle velocity.
For the case with the neutral steer characterized vehicle no adjustments to the rear axle stiffness were necessary, as the vehicle and tyre parameters stated in Table A.1 already result in neutral steering behaviour.

Solving the steady state solution and visualizing the outcome in phase plane diagram form results in Figure 3.6. Here three equilibria can be recognized that are very similar to the ones that were found for the vehicle with understeer characteristics. The only recognizable difference is that the slip angle β at the drift equilibria is greater for the vehicle with understeering behaviour than for the vehicle with neutral steering behaviour.

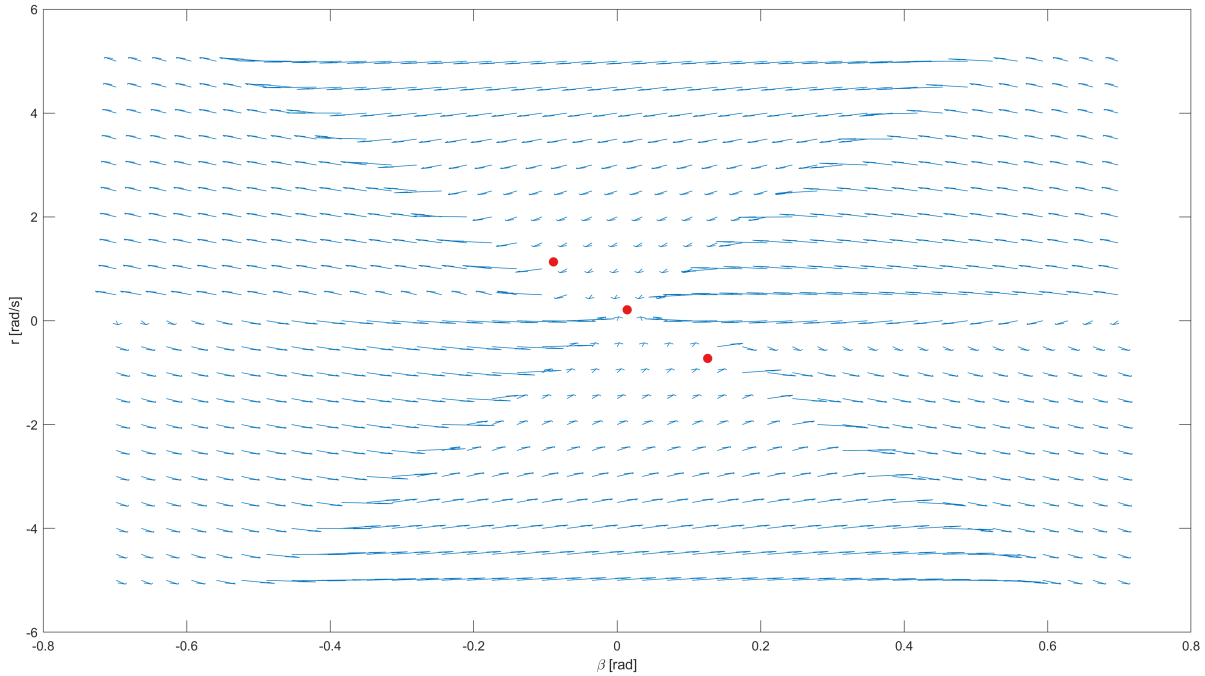

Figure 3.6: Steady state solution for drift equilibria, using Dugoff tyre model and a neutral steering behaviour, visualized in a phase plane diagram.

3.2.3. Oversteer

Driving on a curved road with increasing vehicle velocity, a vehicle that is characterized by oversteer behaviour should decrease the steering angle δ in order to stay on the curvature.
In this case the rear axle stiffness was decreased by 30% in order to give the vehicle oversteer characteristics. Visualizing the outcome of the aforementioned steady state solution using a phase plane

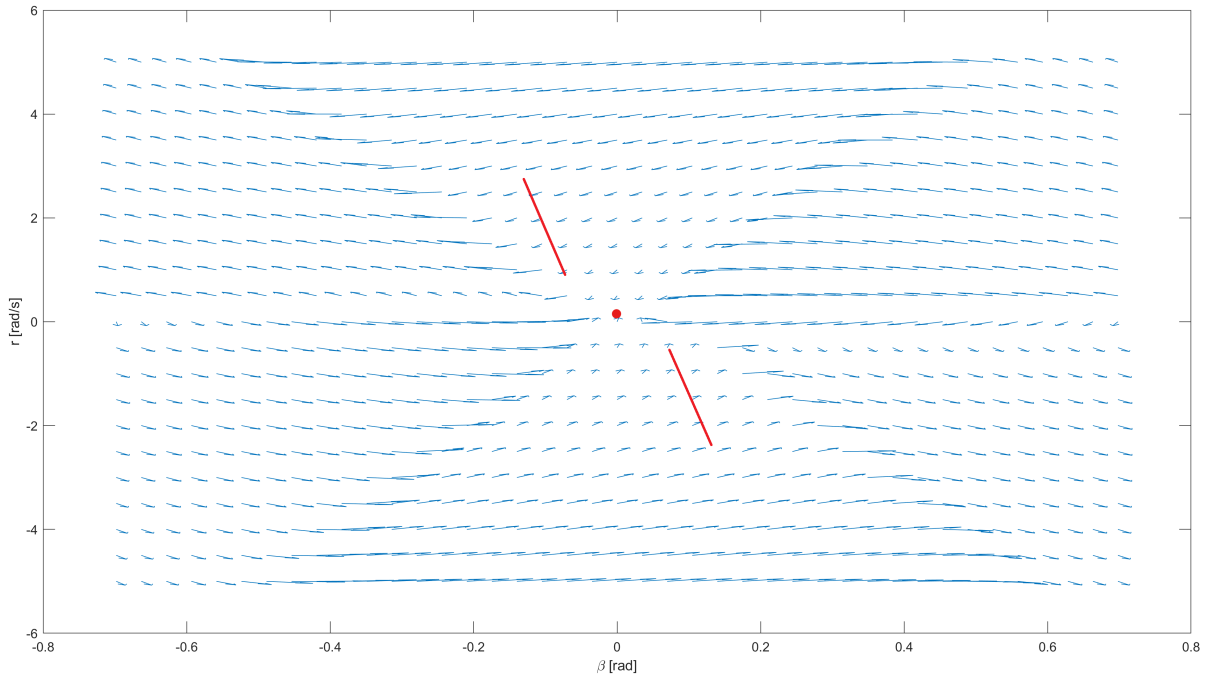

Figure 3.7: Steady state solution for drift equilibria, using Dugoff tyre model and oversteering characteristics, visualized in a phase plane diagram.

diagram results in Figure 3.7. The figure shows one equilibrium point, for typical cornering, in the mid-

dle of the diagram. Furthermore, two ranges of drift equilibria can be distinguished in the phase plane representation, as was found in [22]. The drift equilibria ranges are visualized by the red lines in the figure. It seems that this behaviour exclusively occurs for a vehicle that is characterized by oversteer.

3.3. Different Tyre Models

3.3.1. Linear Tyre Model

As can be seen in the tyre force visualization of Figure 2.4, the Linear Tyre Model assumes the tyre is always in its linear state. As a consequence the longitudinal and lateral forces on the axles of the vehicle are theoretically unlimited with increasing slip angles. Solving the steady state solution as explained in Section 3.1.2 while utilizing the Linear Tyre Model result in the phase portrait shown in Figure 3.8. As

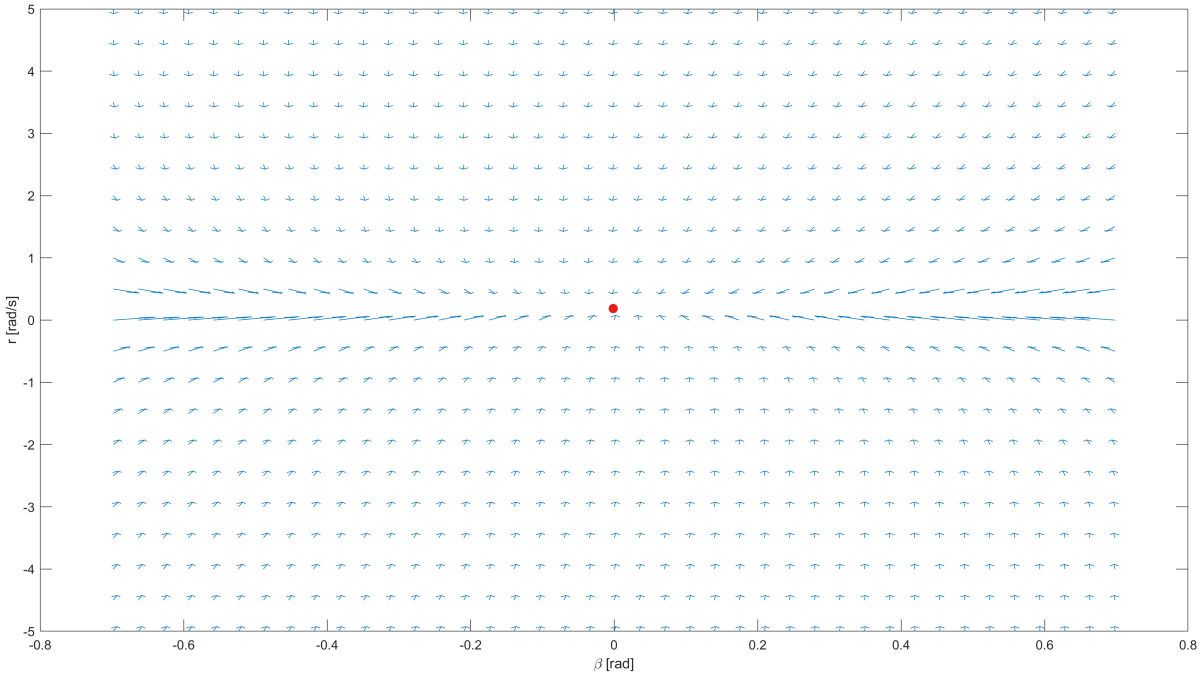

Figure 3.8: Steady state solution for drift equilibria, using Linear tyre model and a neutral steering behaviour with initial conditions as shown in Figure 3.3, visualized in a phase plane diagram.

can be seen in Figure 3.8, all arrows eventually point towards the center red dot. This shows that for every combination of yaw rate r and Slip angle β the tyres of he vehicle are behaving within their linear region. Due to the fact that drift equilibria occur in the non-linear tyre handling range, no drift equilibria can be found using this tyre model. This statement is supported by Figure 3.8, where no drift equilibria can be distinguished.

3.3.2. Dugoff Tyre Model

The tyre force diagrams of the Dugoff Tyre Model in Figure 2.4 show both the linear and non-linear tyre behaviour. The peaks at high slip angles for lateral and longitudinal force (F_y and F_x respectively) indicate a different variant of cornering than conventional cornering. The result of solving the steady state solution while using the Dugoff Tyre Model is shown in Figure 3.6.
As mentioned before, three equilibria can be distinguished from this figure. One in the centre of the graph for conventional cornering, i.e. the tyres of the vehicle are within their linear region. The other two equilibria are drift equilibria, where the tyres are behaving in their non-linear region.

Comparing this method of finding the drift equilibria to the one where the linear tyre model is used, result in a quite obvious conclusion. With the use of the Dugoff tyre model all equilibria, conventional and drifting, could be found, whereas only the equilibrium for conventional cornering could be found with the use of the linear tyre model.

3.3.3. Pacejka Tyre Model (Magic Formula)

The Magic Formula model has the highest values in Figure 2.4 for both the peak longitudinal force F_x as the peak lateral force F_y in the nonlinear region of the tyre. As is the case for the Dugoff tyre model, these peaks indicate a different variant of cornering than conventional cornering. This statement is endorsed by solving and visualizing the steady state solution, which results in the phase portrait shown in Figure 3.9. In Figure 3.9 the equilibrium for conventional cornering is visualized by a red dot in the

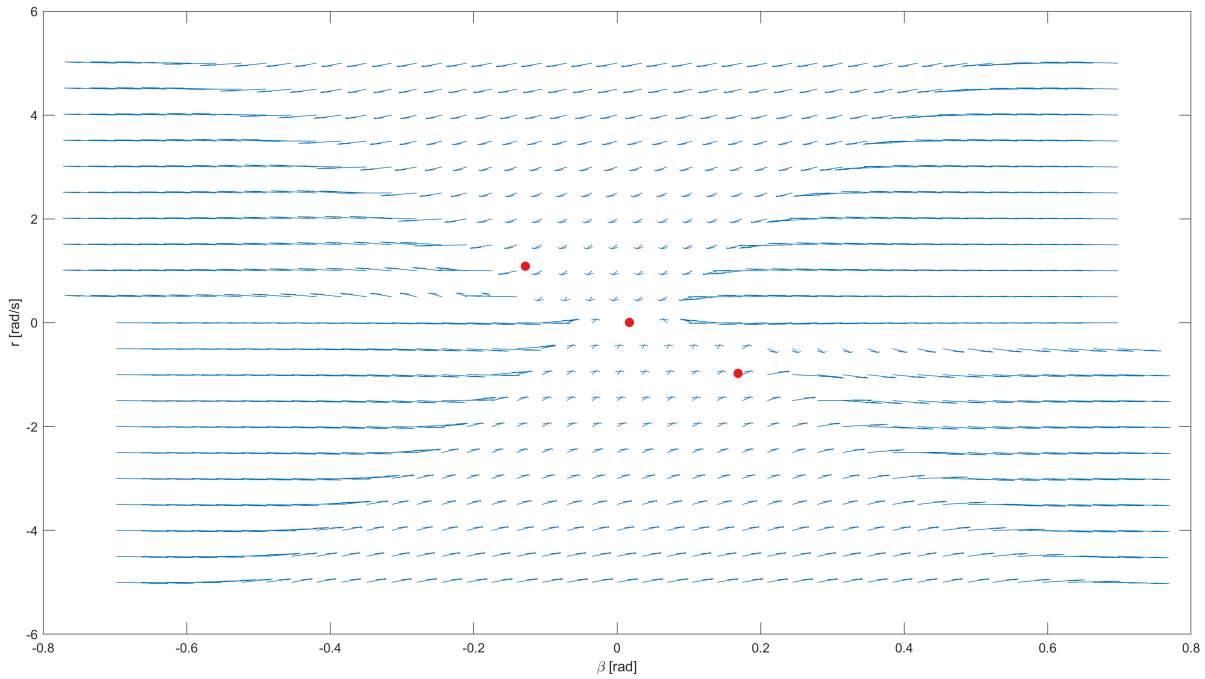

Figure 3.9: Steady state solution for drift equilibria, using Magic Formula model and a neutral steering behaviour, visualized in a phase plane diagram.

centre of the phase plane representation. The other two red dots represent the drift equilibria.

Although the yaw rate at which the drift equilibrium occurs is similar to the method where the Dugoff tyre model was used, the slip angle is not. This can be due to the fact that the Magic Formula Model reaches a higher peak in longitudinal and lateral axle forces than the Dugoff tyre model, as seen in Figure 2.4. The comparison between the outcome of the Magic Formula Model and the Linear tyre model is very similar to that of the comparison between the Dugoff tyre model and the Linear tyre model. Using the Magic Formula model all three equilibria, two for drifting and one for conventional cornering, were found, whereas only the equilibrium for conventional cornering could be found with the use of the linear tyre model.

3.4. Summary

Chapter three shows the theory on how the stability analysis is performed to find drift equilibria in general and for various types of steering behaviours and tyre models. First the general principles on the discovery of drift equilibria are explained. The next section shows the specific approach on how to find and visualize these equilibria. This is done by using a grid of initial conditions for values of the yaw rate r and slip angle β. The steady state solution is then solved in combination with the mathematical descriptions from Chapter 2. The results are then visualized using phase portraits, from which equilibria can be distinguished. The three equilibria that are visualized are two unstable drift equilibria and one stable conventional cornering equilibrium.

The second section of this chapter elaborates on the three different steering characteristics, understeer, neutral steer and oversteer, and makes a comparison. First the conditions of these steering characteristics are explained. Next the drift equilibria, if any, are individually shown for a vehicle that is characterized by understeer, neutral steer or oversteer. Here the Dugoff tyre model is used as the tyre

model.
Drift equilibrium points were found for the vehicles that were characterized by understeering and neutral steering behaviour. However, for the oversteering vehicle, a drift equilibrium range occurs.

In the final section the three tyre models that are described in Chapter 2 are used to find drift equilibria and are compared to each other. For the linear tyre model only one equilibrium, for conventional cornering, could be found. Using the Dugoff tyre model and the Magic Formula Model all three equilibria could be found. The main difference between the outcome of the two latter tyres models is that the slip angles β at which the drift equilibria occur are greater for the steady state solution where the Dugoff model was used than where the Magic Formula Model was used. Solving the steady state solutions in this last section was done using a neutral steering vehicle.

4

Drift equilibria

In order to be able to control a vehicle towards drifting behaviour, a single drift equilibrium point or plane, as described in Chapter 3, will be too limited. Eventually a lookup table containing a full range of drift equilibria has to be determined offline, containing all possible drift equilibria for an applicable vehicle, as was partly done in [33]. The reason for this is that the full spectrum of autonomous drifting can then be utilized, of which the relevance is explained in the introduction of this report.

In this chapter the biggest novelty of the report is shown, as drift equilibria ranges are set up for the vehicle which parameters are shown in Table A.1. First, certain vehicle parameters are varied in order to investigate the influence this has on the drift equilibria. The parameters that are varied are the location of the centre of gravity, the mass and the tyre cornering stiffness. Each of the variables is varied by -30% to $+30\%$ in five steps. This way values are achieved that all lay in the range of commercial passenger vehicles. Calculating and visualizing this range in five steps is done in order to be able to calculate the drift equilibria over the full -30% to $+30\%$ range, while maintaining a clear distinction between the calculation. As a result it becomes more straightforward to discuss the achieved results. In the final section of this chapter two different tyre models are considered to achieve the drift equilibria. The tyre models that are considered are the Dugoff tyre model and the Magic Formula model. The Linear tyre model is not considered as no drift equilibria can be found using this tyre model, as shown in Chapter 3.

For the aforementioned cases the Matlab function `fsolve` has been used, which is a dedicated tool to solve a system of nonlinear equations. This function incorporates the Levenberg-Marquardt algorithm. The algorithm can be tuned by adjusting the initial Levenberg-Marquardt parameter. Although `fsolve`, which is a gradient based solver, is not always able to automatically find global minima, each equilibrium set can be found by tuning an initial guess and by performing multiple searches. Tuning the initial guess proved to be essential in some cases for finding drift equilibria. The `fsolve` function has been placed in a loop where it is solved for vehicle velocity values of $[1:100]$ m/s, starting at 1 m/s and increasing with every step in the loop. This range for the vehicle velocity was chosen as it covers the majority of possible velocities of commercial passenger vehicles. The initial conditions x_0 that were used by the solver are given by:

$$x_0 = \begin{bmatrix} v_x & v_y & \omega & \delta & T_{net} \end{bmatrix} = \begin{bmatrix} \frac{V_0}{2} & -\frac{V_0}{2} & 25 & -0.8 & 3000 \end{bmatrix} \tag{4.1}$$

where V_0 and ω describe the velocity of the current loop step and the angular wheel velocity respectively. The longitudinal velocity is described by v_x and the lateral velocity is described by v_y. Finally, δ and T_{net} respectively describe the steering angle and the net torque applied to the rear axle. These values were based on the initial conditions used in [33]. Furthermore they were tuned in order for the solver to find global minima. Intuitively, the initial condition for the wheel rotational velocity ω could be set using Equation 2.17. This equation however describes the wheel rotational velocity in the linear tyre region. As the tyres are saturated during drifting, and are therefore behaving in their non-linear range, this equation can not be used to obtain an initial condition for ω. Also intuitively, the initial condition for the lateral velocity v_y should be considerably lower than the initial condition for the longitudinal velocity

v_x. Considering the drift equilibria found in Chapter 3 and utilizing the equation for the sideslip angle (Equation 4.2), it would be expected that the initial condition for the lateral velocity should be at about $\frac{1}{10}$th of the initial condition for the longitudinal velocity.

$$\beta = \arctan(\frac{v_y}{v_x}) \approx \frac{v_y}{v_x} \tag{4.2}$$

However, by tuning, the most global minima were found for the initial condition of v_y as shown in initial conditions (4.1).

All simulations have been performed using the Dugoff tyre model, with tyre stiffnesses obtained as shown in Equation 2.24. The cornering radius is set to a fixed value of $R = 30$ m. Finding drift equilibria for various cornering radii, albeit exclusively with the Magic Formula model, has been performed in [33].

4.1. Varying Vehicle Parameters

In this section three different vehicle parameters are varied. These are the location of the centre of mass of the vehicle, the mass of the vehicle and the tyre stiffnesses. These particular parameters are selected for three reasons. First, these parameters have a direct influence on the simulations as they are directly mathematically implemented in the Dugoff tyre model. As a result a clear comparison can be made between the outcomes of the varying vehicle parameters. Second, these parameters are chosen as they make up the core vehicle properties. The mass and centre of gravity of commercial passenger vehicles varies for almost every individual model. Additionally a wide variety of tyres are available for commercial vehicles. Therefore these three vehicle parameters present themselves as core vehicle properties. Third, the mass and centre of gravity of a vehicle change when the vehicle is being loaded. Adding e.g. passengers and luggage to a vehicle increases the total mass and could change the location of the centre of gravity. The latter could for example be caused by passengers in the rear seats. As for the tyre stiffnesses, tyre selection could vary over the lifespan of a vehicle.

4.1.1. Vehicle Geometry

The vehicle geometry is varied by running simulations where the centre of gravity is moved more to the front or more to the back of the vehicle. The distance from the front axle to the centre of gravity, described by l_f, is made leading for these simulations. The lower the value for l_f, the closer the centre of gravity of the vehicle is to the front axle. The distance from the rear axle to the centre of gravity, described by l_r, is then given by:

$$l_r = L - l_f \tag{4.3}$$

Where L is determined beforehand by using the values for l_f and l_r from Table A.1 and the equation:

$$L = l_f + l_r \tag{4.4}$$

As a result the values that are used to vary the vehicle geometry are given by:

$$\begin{bmatrix} l_f \\ l_r \end{bmatrix} = \begin{bmatrix} 1.6681 & 2.0255 & 2.3830 & 2.7404 & 3.0979 \\ 3.1449 & 2.7875 & 2.4300 & 2.0726 & 1.7151 \end{bmatrix} \tag{4.5}$$

Running the simulation while using each column of these values as an input for the solver for every step of the loop, results in Figure 4.1. What stands out is that not for every location of the centre of gravity a solution is found. This is the case when the centre of gravity is shifted 30% towards the rear axle. However, a solution is found for the case when the centre of gravity is shifted 23% towards the rear axle. It therefore seems that a problem keeps the solver from finding solution for values greater than 23% above the baseline l_f. The fact that no solution is found for the $+30\%$ case could have several reasons. First, it could be that for this particular vehicle geometry, or for cases larger than $+23\%$, no drift equilibria can be found. Second, it could be caused by the solver finding only local minima and not global minima, where only the latter results in a complete solution. This in turn could be caused by insufficient tuning of the solver, despite the performed tuning efforts.

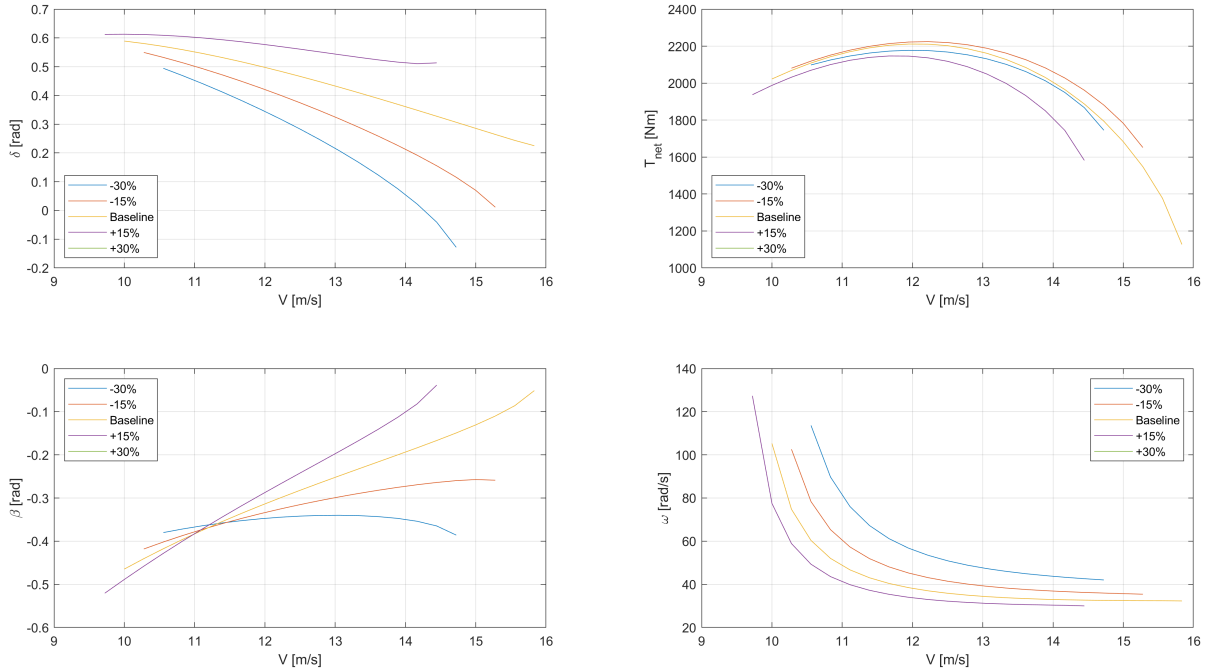

Figure 4.1: Drift equilibria results for the vehicle parameterized by Table A.1, with varying location of the centre of gravity.

In the top left graph of Figure 4.1 the steering angles δ that are necessary to maintain a drifting motion are plotted against their respective velocities. As can be seen, a direct relationship exists between the steering angle gain and the location of the centre of gravity. In other words, the necessary steering angle decrease with increasing vehicle velocity decreases when the location of the centre of gravity is shifted more to back of the vehicle. It increases when the location of the centre of gravity is shifted more to front of the vehicle. This can be declared by the change in understeer gradient given by Equation 3.6 and the related steering angle given by Equation 3.5.
The top right graph of Figure 4.1 shows the net rear axle torque T_{net} for the found drift equilibria, plotted against the vehicle velocity V. From this graph it shows that the toque curves for all cases only differ marginally. Only for the case where the centre of gravity is shifted 15% towards the rear axle, the necessary torque for drifting is somewhat lower. As the torque curves in this part of the figure are relatively close to each other, it is assumed that their marginal differences are caused by solver settings. Modern commercial passenger vehicle engines can not generate the amount of torque displayed in this graph. To reach these net rear axle torque values, the gear ratios of a vehicle gearbox should be utilized.
The vehicle slip angle β is plotted against the vehicle velocity V in the bottom left of the figure. Here is it visible that the slip angle gain with increasing vehicle velocity is different with each parameter of the centre of gravity. A direct relationship exists between the slip angle gain and the relative shift of the location of the centre of gravity, i.e. the slip angle gain increases when the location of the centre of gravity is placed more towards the rear axle of the vehicle.
In the final graph of Figure 4.1, located at the bottom right, the wheel rotational velocity ω is plotted against the vehicle velocity V. Here an inverse relationship exists between the wheel rotational velocity and the location of the centre of gravity. In other words, for a given vehicle velocity, a higher wheel velocity is necessary for each decreasing step of the location of the centre of gravity. However, with increasing vehicle velocity, these differences become marginal.

4.1.2. Vehicle Mass

Simulations have been performed where the mass of the vehicle has been varied from -30% to $+30\%$, with regards to the baseline as well. The baseline is stated in Table A.1. As a result the input for this simulations is as follows:

$$m = \begin{bmatrix} 1115.2 & 1354.2 & 1593.1 & 1832.1 & 2071.1 \end{bmatrix} \tag{4.6}$$

Figure 4.2 is the result of the simulation where for each loop step one of the values of 4.6 has been used. Here the solver did succeed in converging towards solutions for the five different mass inputs.

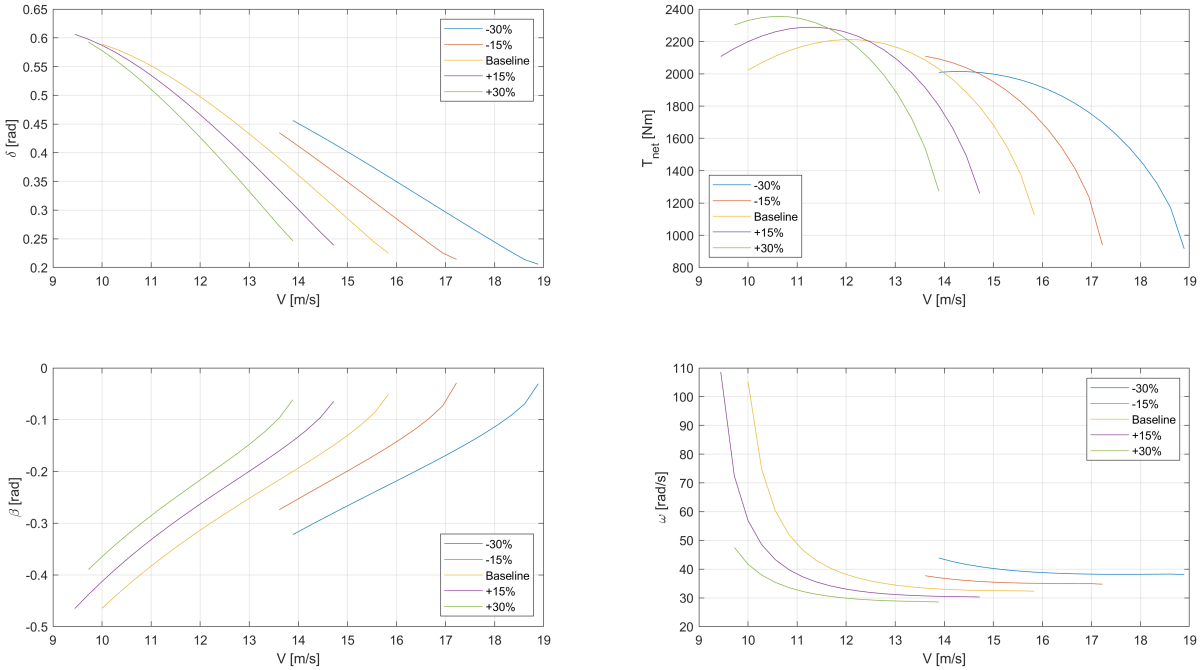

Figure 4.2: Drift equilibria results for the vehicle parameterized by Table A.1, with varying vehicle mass.

In the top left graph of Figure 4.2, an inverse relationship is shown between the steering angle δ and the vehicle velocity V. In other words, with increasing vehicle mass, a decrease of steering angle is necessary to maintain the vehicle in a drifting state.
The net torque applied to the rear axle T_{net} is shown in the top right of the figure, plotted against the vehicle velocity V. Here it can be seen that a shift in the torque curve occurs for varying mass. The vehicle with the highest mass is able to perform a drifting motion at lower vehicle velocities than vehicles that are lower in weight. Furthermore, less rear axle torque is necessary with decreasing vehicle mass. This can be declared by the fact that a lighter vehicle has less normal force F_z acting on the tyres. As the normal force has a direct relationship with the forces acting on the tyres, a lower normal force means that the tyre can be saturated with a lower amount of torque.
In the bottom left of the figure a shift in sideslip angle can be observed. Here the vehicle sideslip angle β is plotted against the vehicle velocity V. For the same values for the vehicle velocity, the slip angles are lower for the cases where the vehicle mass is higher, i.e. an inverse relationship exists.
The bottom right graph of the figure shows the wheel rotational velocity ω plotted against the vehicle velocity V. Here it can be seen that with increasing weight, the wheel rotational velocity necessary to keep the vehicle drifting state decreases. This difference does dampen out with increasing vehicle velocity.

4.1.3. Cornering Stiffness

For this section simulations were performed where the rear cornering stiffness $C_{\alpha r}$ was the varying parameter. In real life application this can be seen as replacing the rear tyres by ones with different specifications. As in this report the longitudinal tyre stiffness is calculated by $C_\kappa = 1.2 * C_\alpha$, varying the rear lateral tyre stiffness affects the rear longitudinal tyre stiffness as well. The tyre stiffnesses that are used for the simulation are then given by:

$$\begin{bmatrix} C_{\alpha f} \\ C_{\alpha r} \\ C_{\kappa f} \\ C_{\kappa r} \end{bmatrix} = \begin{bmatrix} 157810 & 157810 & 157810 & 157810 & 157810 \\ 108331 & 131544 & 154758 & 177972 & 201185 \\ 189372 & 189372 & 189372 & 189372 & 189372 \\ 129997 & 157853 & 185709 & 213566 & 241422 \end{bmatrix} \tag{4.7}$$

Where each column of this set is used for each step of the simulation loop. As a result of the varying tyre stiffnesses, the understeer gradient varies as well, resulting in the following values for K_{us}:

$$K_{us} = \begin{bmatrix} -0.0214 & -0.0088 & 0 & 0.0065 & 0.0115 \end{bmatrix} \tag{4.8}$$

From these values of the understeer gradient, it can be seen that the vehicle ranges from oversteering behaviour ($K_{us} < 0$), to neutral steering behaviour ($K_{us} = 0$), to understeering behaviour ($K_{us} > 0$).

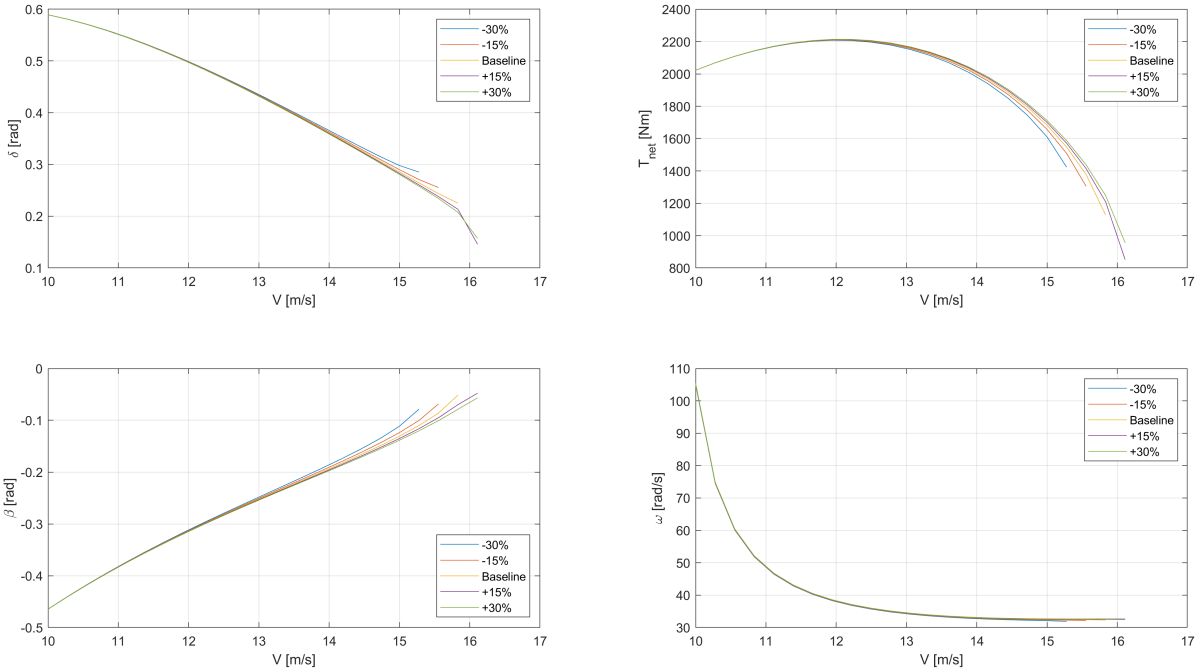

Figure 4.3: Drift equilibria results for the vehicle parameterized by Table A.1, with varying cornering stiffnesses.

Figure 4.3 shows the result of the simulation where for every loop the cornering stiffnesses are set as shown in (4.7).
The steering angle δ is plotted against the vehicle velocity V in the top left of this figure. What immediately stands out, and this goes for all graphs in Figure 4.3, is that the results of the varying stiffnesses is very similar. This can be declared by the fact that the vehicle behaves very similar when exposed to the small changes in the understeer gradient K_{us} at the velocities V for which drift equilibria are found. This statement is supported by Figure 3.4. This figure also explains the outcome differences of the simulation at higher velocities, as these then become more distinguishable.
For each of the outcomes of the top left graph of the figure, an inverted relationship exist between the vehicle velocity V and the steering angle δ. Furthermore, at higher velocities it becomes clear that for lower rear tyre stiffnesses, a higher steering angle is necessary to obtain a drift equilibrium, and vice versa.
The top right graph in Figure 4.3 shows the net torque applied to the rear axle T_{net}, plotted against the vehicle velocity V. Here the differences between the varied tyre stiffnesses only become visible at higher velocities as well. Here it can be seen that for higher tyre stiffnesses, a higher amount of net rear axle torque is necessary to obtain drift equilibria. Therefore there is a direct relationship between the tyre stiffness and the necessary net torque that is applied to the rear axle.
In the bottom left graph of the figure the vehicle sideslip angle β is plotted against the vehicle velocity V. From this graph it can be seen that the sideslip angles increases as the vehicle velocity increases. At higher velocities the differences between the varied rear tyre stiffnesses are more distinguishable. With increasing rear tyre stiffness, the vehicle slip angle becomes smaller for the same respectable velocities. In the final graph of Figure 4.3, located at the bottom right, the wheel rotational velocity ω is plotted against the vehicle velocity V. Here the outcome of the simulation seems to be the same for all five cases. However, zooming in on this graph, a small difference can be distinguished between the cases at higher velocities. At higher rear tyre stiffnesses, the wheel rotational velocity is higher, and

vice versa.
Although the differences for the cases considered in Figure 4.3 are marginal, the figure does show the increasing difference in simulation outcome with increasing vehicle velocity.

4.2. Varying Tyre Model

In order to investigate the influence of the tyre model on the drift equilibria, the drift equilibria are set up using two different tyre models in this section. This is also done using the Matlab `fsolve` function and with the initial values as described in (4.1). Furthermore, the vehicle parameters as stated in Table A.1 are used.

The tyre models that will be considered are the Dugoff tyre model and the Magic Formula model. The linear tyre model will not be considered in this section, as it was shown in Chapter 3 that no drift equilibria could be found using this tyre model. The tyre parameters for the implementation of the Magic Formula model are listed in Table A.2. The tyre stiffnesses for the Dugoff tyre model are calculated as described in Equation 2.24.
In Chapter 3 it was already shown that differences in drift equilibria exist for these tyre models. In this section the full range of drift equilibria will be considered. Running the simulation for both tyre models and visualizing the outcome, results in Figure 4.4. In this figure, all graphs are plotted against the

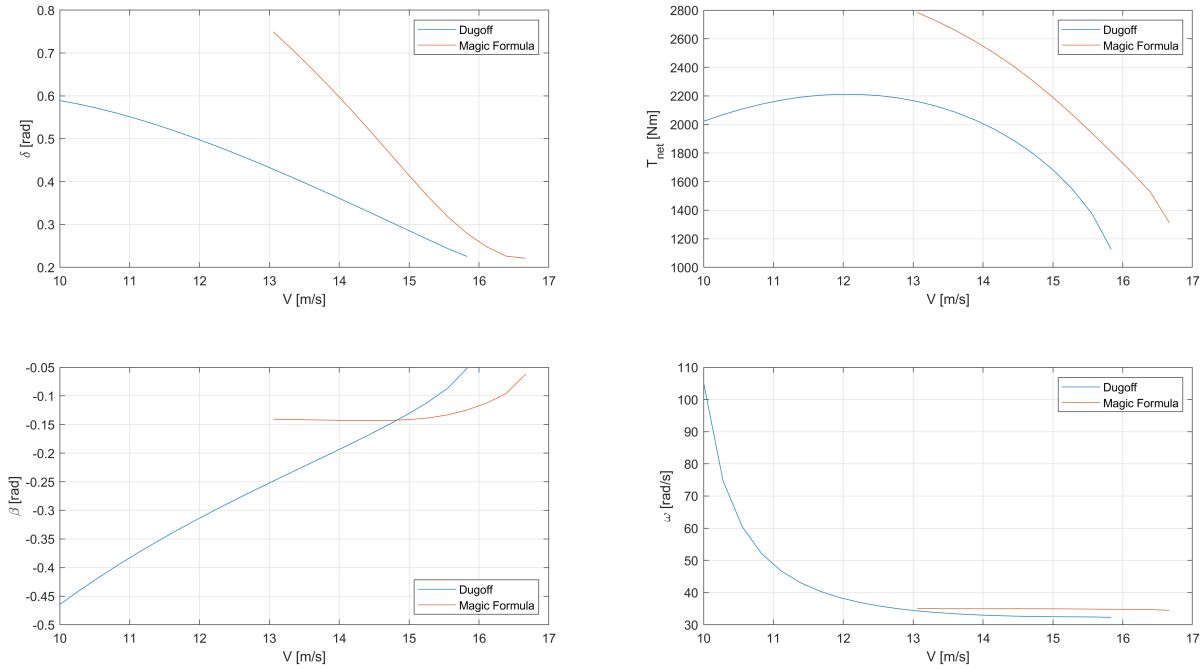

Figure 4.4: Drift equilibria results for the vehicle parameterized by Table A.1, for Dugoff tyre model and Magic Formula model.

vehicle velocity V, which will be represented at the horizontal axle for each of the graphs.
In the top left graph of the figure, the steering angle δ is shown for the two cases. For both tyre models an inverse relation exists considering the steering angle and the vehicle velocity. With increasing velocity, the steering angle decreases. Furthermore, the solution using the Dugoff tyre model indicates that the steering angle should be smaller than for the case where the Magic Formula model was used, for the same respective velocities. Finally it seems that the range of drift equilibria that were found using the Dugoff tyre model is larger than for the other tyre model. This could however also been caused by the solver settings, indicating a convergence issue.
In Figure 4.4, in the top right half, the net rear axle torque T_{net} is visualized. Here it is shown that the necessary torque for drift equilibria using the Magic Formula model is higher than when applying the Dugoff tyre model. Also drift equilibria are found at higher vehicle velocities when using the Magic Formula model. Furthermore, for the case where the Dugoff tyre model is used, the torque curve first rises with increasing vehicle velocity and then decreases as the velocity goes above $V \approx 12$ m/s. On the other hand the Magic Formula model only shows a decreasing value for T_{net} with increasing V.

The bottom left graph of the figure shows the vehicle slip angle β. From this graph it becomes clear that using the Dugoff tyre model, an almost linear decrease in slip angle is found with increasing vehicle velocity. The slip angles that are found using the other tyre model seem much more stable, almost even constant for velocities between $V \approx 13$ m/s and $V \approx 15$ m/s. Using the Dugoff tyre model, higher vehicle sideslip angles are determined up to the point that the lines of the two methods cross. From there on, with increasing vehicle velocity, the determined slip angle of the Magic Formula model becomes higher. In the graph at the bottom of Figure 4.4, the wheel rotational velocity is displayed for both cases. Here it is shown that the Dugoff tyre model indicates an exponential decrease in wheel rotational velocity with increasing vehicle velocity, on the left side of this graph. This decrease damps out for velocities of $V > 14$ m/s, from which the wheel rotational velocity seems to stay constant. For the Magic Formula model, the wheel rotational velocity seems constant over the whole drift equilibria range.

4.3. Summary

In this chapter the influence of varying vehicle parameters on the drift equilibria is shown, together with a comparison between two tyre models for determining the drift equilibria.
First the solver, the initial values and the boundary values were elaborated on. The Matlab function `fsolve` has been used to solve the set of non-linear equations.

In the next section certain vehicle parameters were varied compared to set baseline values by -30% to $+30\%$ in five steps. The parameters that were considered are the location of the centre of gravity of the vehicle, the mass of the vehicle and the cornering stiffness of the rear tyres. For each of these three cases, drift equilibria were determined. Next, for each individual varying parameter relationships were found and discussed regarding the steering angle, net rear axle torque, vehicle sideslip angle and wheel rotational velocity. All with regard to the vehicle velocity.

In the final section of this chapter the Dugoff tyre model and the Magic Formula model are considered for determining drift equilibria. The same relationships as in the previous section are discussed.

5

Conclusions & Recommendations

5.1. Conclusions

As an addition to current safety systems, research is performed in order to develop systems that rely on autonomous drifting. Properly controller, drifting can increase vehicle safety, autonomous driving acceptance and vehicle performance. During a drifting motion, a vehicle negotiates a corner while maintaining relatively large sideslip angles. During this motion the rear tyres are saturated.

A review of the state of the art showed a method that enables the generation and visualization of drift equilibrium points. To be able to use this method, an understanding of the fundamental mathematics of vehicle and tyre behaviour is essential. A three state vehicle model suffices for generating the drift equilibria. Furthermore, the linear tyre model, Dugoff tyre model and Magic Formula model are mathematically considered. To gain insight on the differences between these three tyre models, the forces acting on the tyres for each tyre model type can be visualized. From this diagram the tyre behaviour for different longitudinal slip and lateral slip angles for each of these tyre models can be compared.

Determining the drift equilibria is done by solving the steady state solution. The steady state solution is set up using the fundamental mathematical equations and a grid of initial conditions. The result of this solution can be visualized in a phase plane representation, giving insight for which values of yaw rate and vehicle sideslip angle drift equilibria occur. This phase plane representation shows the yaw rate and sideslip angle location for conventional cornering as well, resulting in a total of three equilibria.
Using this method, the influence of different steering characteristics on drift equilibria can be investigated. These steering characteristics are divided intro three types, understeer, neutral steer and oversteer. Switching between these steering characteristics while maintaining the same values for the rest of the vehicle and road parameters can be done by varying the rear lateral cornering stiffness. Using the Dugoff tyre model, three equilibria are found for the understeering vehicle, of which two are drift equilibria. The other equilibrium indicates conventional cornering. The same amount and types of equilibria can be found for a vehicle that is characterized by neutral steer. For an oversteering vehicle however, one equilibrium is found for conventional cornering and two equilibrium ranges are found for drifting. Therefore an oversteering vehicle has a range of vehicle states yaw rate and sideslip angle for which drifting is possible. For understeering and neutral steering vehicles, this is limited to drift equilibrium points.
Various tyre models could be used in order to identify drift equilibria for a vehicle with neutral steering behaviour. However, those can not be found using the linear tyre model, as for all inputs of yaw rate and sideslip angle the vehicle will be directed towards stable conventional cornering. With the use of the Dugoff tyre model all three equilibria, of which two are drift equilibria, can be identified. The same goes for the Magic Formula model. The main difference in the results of using this tyre model compared the Dugoff model is that the drift equilibria were found at higher sideslip angles for the Magic Formula model. This is caused by the higher possible peak values for the longitudinal and lateral axle forces of the latter model.

The values that parameterize a vehicle have a direct influence on the drift equilibria. Shifting the centre of gravity towards the back of the vehicle increases the steering angle that is necessary to maintain

a drifting motion. This shift also results in a steeper sideslip angle gain and lower wheel rotational velocities. The opposite is true for the cases where the location of the centre of gravity of the vehicle is shifted more to the front axle.
Decreasing the mass of the vehicle leads to higher steering angles, lower sideslip angles and equilibria at higher velocities for drifting. The net rear axle torque decreases in this case as well, while the necessary wheel rotational velocity increases. An increase in the mass of the vehicle leads to opposite results.
The difference in cornering stiffnesses, and thereby the differences in steering behaviour, only comes forward at relatively high velocities. Using a cornering radius of thirty meters and analysing its resulting drift equilibria, the differences between the cases are marginal as these kind of velocities are not reached. Although marginal, at higher velocities a higher steering angle is necessary to obtain a drift equilibrium with decreasing rear tyre stiffness. In this case the net rear axle torque decreases, the sideslip angle becomes larger and the wheel rotational velocity decreases as well.
When the Dugoff tyre model and the Magic Formula model are compared regarding the generation of drift equilibria, several differences emerge. Using the Dugoff tyre model, a larger range of drift equilibria is found. The Magic Formula model does however find these equilibria at higher velocities. Furthermore, the results achieved utilizing the Dugoff model show a torque curve with increasing velocity, whereas the other considered tyre model shows an almost linear net rear axle torque decrease. The tyre models show similar behaviour for the steering angle with increasing vehicle velocity. Finally, the determined sideslip angle and the wheel rotational velocity differ, as these values decrease for the Dugoff tyre model. For the Magic Formula model these stay constant with increasing velocity, apart from a slight decrease in sideslip angle at higher velocities.
In conclusion, a variety of vehicle and tyre parameters were investigated, together with several tyre models. Each of these aspect influence the parametric location of the drift equilibria and its behaviour. Therefore, in order to construct a reliable reference point for, for example, future implementation, these influences have to be taken into account.

5.2. Recommendations

The drift equilibrium analyses that are performed in this thesis are limited by the chosen vehicle model, varying parameters and used tyre models. Therefore recommendations should be made in order to expand the research and knowledge on drifting.
First the missing drift equilibria for the case where the centre of gravity of the vehicle is shifted 30% to the rear axle could be investigated. This can be done by investigating in two directions. First, vehicle geometries at which drifting equilibria can not exist could be researched. The second research direction can be focused on the solver. The solver used in this research could be extensively tuned to try and find a solution for the missing case. Another possibility could be to utilize a more stable algorithm to find the global minima. Lastly, in stead of the used solver a numerical approach could be utilized to find the drift equilibria.

Additionally, the following further research could be performed:

1. **Expand the used methods and parameters**
   Due to the fact that this research is limited by the chosen vehicle model, varying parameters and used tyre models, research should be performed on the effect of other varying parameters and models. In the first place the vehicle model could be expanded by using one that incorporates roll, pitch and yaw motion. Suspension dynamics could also be included. Additionally, different tyre models and additions like Delft Tyre could be considered, including tyre transient behaviour. Using more complex vehicle and tyre models makes for even more vehicle and road parameters that can be investigated regarding drifting behaviour.

2. **Tyre force estimation**
   In this research tyre models are used in order to determine the forces acting on the tyres. These forces are then used to determine the drift equilibria. However, different methods could be considered to determine the forces acting on the vehicle. One of these methods is the load sensing bearing, which directly measures the acting forces without the use of a tyre model.

3. **Controller and plant simulation**
   After a solid drifting analysis has been performed, the found equilibria could be set as reference

values for plant simulation. The vehicle model that represents this plant could, for example, be simulated using a model in Simulink or by using IPG Carmaker. A controller should be added in order to run the plant simulations, guiding the vehicle towards and keeping it at the drift equilibria. Literature described various types of controllers including linear quadratic regulator control and model predictive control. For the latter control type, tools like ACADO or FORCESPRO could be used.

4. **Physical experiment**
   Finally a physical experiment in real world conditions could be performed. This way the theoretical research can be evaluated with physical experimental data. Using this data the theoretical research can be tuned, which could result in an even broader understanding of drifting.

A

Appendix A: Parameters

Table A.1: Vehicle and road parameters used to create the phase plane representation shown in Figure 3.6. The vehicle values are of a Porsche 911, extracted from IPG Carmaker [33].

Symbol	Value	Unit	Description
l_f	2.383	m	Distance from front axle to CoG
l_r	2.43	m	Distance from rear axle to CoG
m	1593.12	kg	Vehicle Mass
I_z	2575.9	kg*m^2	Vehicle moment of inertia about vertical axis
C_κ	94686	N/[-]	Longitudinal slip stiffness per wheel
$C_{y,f}$	78905	N/rad	Front cornering stiffness per wheel
$C_{y,r}$	77379	N/rad	Rear cornering stiffness per wheel
μ_0	1	[-]	Peak road friction coefficient
e_r	0.01	[-]	Road adhesion reduction coefficient
I_s	17	[-]	Steering ratio
g	9.81	m/s^2	Gravitational acceleration
r_ω	0.508	m	Wheel radius
I_ω	3.916	kg*m^2	Wheel inertia

Table A.2: Pacejka tyre model parameters for a tyre with non-convex slip properties as used in [33].

Tyre Parameter	Value
B	6.8488
C	1.4601
D	1
E	-3.6121

Bibliography

[1] M. Acosta. “PhD Automotive Engineering Progress Report: Research on Multi-Actuated Agile Electric Vehicles: A Drift-based approach to Last-Moment Accident Avoidance Manoeuvres on Loose Surfaces”. PhD thesis. Coventry University, 2017.

[2] M. Acosta. “Vehicle Dynamics Virtual Sensing and Advanced Motion Control for Highly Skilled Autonomous Vehicles”. PhD thesis. Technischen Universität Ilmenau, 2019.

[3] M. Acosta and S Kanarachos. “Highly Skilled Autonomous Off-Road Vehicles”. In: Automotive Electronics Innovation (AESIN) Conference (2017), pp. 1–22.

[4] D. Ammon. “Vehicle dynamics analysis tasks and related tyre simulation challenges”. In: Vehicle System Dynamics : International Journal of Vehicle Mechanics and Mobility 43 (2005), pp. 30–47.

[5] Craig E. Beal and J. Christian Gerdes. “Controlling Vehicle Instability through Stable Handling Envelopes”. In: Proceedings of the 2011 ASME Dynamic Systems and Control Conference (2011).

[6] Mingyuan Bian et al. “A Dynamic Model for Tire/Road Friction Estimation under Combined Longitudinal/Lateral Slip Situation”. In: SAE Technical Papers (2014).

[7] Carrie G. Bobier and J. Christian Gerdes. “Staying within the nullcline boundary for vehicle envelope control using a sliding surface”. In: Vehicle System Dynamics (2012).

[8] I. Chakraborty, P. Tsiotras, and J. Lu. “Vehicle posture control through aggressive maneuvering for mitigation of T-bone collisions”. In: Decision and Control and European Control Conference (CDC-ECC) 2011 50th IEEE Conference (2011), pp. 3264–3269.

[9] W. Chesky. Side view of electric suv concept car. iStock.com/cheskyw. 2016.

[10] Henrik Detjen et al. “How to Increase Automated Vehicles’ Acceptance through In-Vehicle Interaction Design: A Review”. In: International Journal of Human–Computer Interaction 37.4 (2021), pp. 308–330.

[11] H. Dugoff, P. Fancher, and L. Segel. “An Analysis of Tire Traction Properties and Their Influence on Vehicle Dynamic Performance”. In: SAE Transactions 79.2 (1970), pp. 1219–1243.

[12] J. Edelmann and M. Plochl. “Handling characteristics and stability of the steadystate powerslide motion of an automobile”. In: Regular and Chaotic Dynamics 14:682–692.10.1134/S1560354709060069 (2009).

[13] Angela H. Eichelberger and Anne T. McCartt. “Toyota drivers’ experiences with Dynamic Radar Cruise Control, Pre-Collision System, and Lane-Keeping Assist”. In: Journal of Safety Research 56 (2016) (2015), pp. 67–73.

[14] E. Fiala. ““Seitenkräfte am rollenden luftreifen”. In: VDI Zeitschrift 96 (1954), pp. 973–979.

[15] A. Gray et al. “Predictive control for agile semi-autonomous ground vehicles using motion primitives”. In: American Control Conference (ACC) (2012), pp. 4239–4244.

[16] C. Hewitt et al. “Assessing public perception of self-driving cars: the autonomous vehicle acceptance model”. In: 24th International Conference on Intelligent User Interfaces (2019).

[17] R. Y. Hindiyeh. “Dynamics and Control of Drifting in Automobiles”. In: PhD Thesis, Stanford University (2013).

[18] Jack Leslie. Drifting VW Polo WRC. 2014. URL: https://www.carthrottle.com/post/VpNnN3/.

[19] LMC. “The outlook for Autonomous Vehicle sales and their impact to 2050”. In: LMC Automotive (2018).

[20] Cathy Morrow.
Automotive manufacturers invest in digitization, autonomous and electric vehicles, Forbes. Apr. 2019. URL: https://www.forbes.com/sites/cathymorrowroberson/2019/03/24/automotive-manufacturers-invest-with-a-focus-on-digitization-autonomous-and-electric-vehicles/?sh=1b61d9a5918b (visited on 04/21/2021).

[21] H. Pacejka. “Tire and Vehicle Dynamics”. In: Elsevier 3rd ed. (2012).

[22] Joop P. Pauwelusssen. Essentials of Vehicle Dynamics. Elsevier, 2015.

[23] B. Pfleging and A. Schmidt. “(non-)
driving-related activities in the car: Defining driver activities for manual and automated driving.” In: Workshop on experiencing autonomous vehicles: Crossing the boundaries between a drive and a ride (2015).

[24] SAE. “SAE J3016 Standard: Taxonomy and Definitions for Terms Related to On-Road Motor Vehicle Automated Driving Systems”. In: SAE (2014).

[25] Sutliff and Stout. Who is At Fault in a T-Bone Car Accident? Apr. 2021. URL: https://www.sutliffstout.com/houston-car-accident-lawyer/fault-t-bone-car-accident/.

[26] D. Tavernini et al. “Minimum time cornering: the effect of road surface and car transmission layout”. In: Vehicle System Dynamics: International Journal of Vehicle Mechanics and Mobility 51(10):1533–1547 (2013).

[27] E. Velenis. “Expert driving techniques at the limit of handling”. In:
Vehicle Dynamics and Control Conference (VDC). (2011).

[28] E. Velenis. “FWD Vehicle Drifting Control: The Handbrake-Cornering Technique”. In:
2011 50th IEEE Conference on Decision and Control and European Control Conference (2011), pp. 3258–3263.

[29] E. Velenis, E. Frazzoli, and P. Tsiotras. “Steady-state cornering equilibria and stabilization for a vehicle during extreme operating conditions”. In:
International Journal of Vehicle Autonomous Systems 8(2–4):217–241 (2010).

[30] E. Velenis and P. Tsiotras. “Minimum time vs maximum exit velocity path optimization during cornering”. In: 2005 IEEE international symposium on industrial electronics (2005), pp. 355–360.

[31] E. Velenis et al. “Stabilization of steady-state drifting for a RWD vehicle”. In:
Proceedings of AVEC (2010).

[32] E. Velenis et al. “Steady-state drifting stabilization of rwd vehicles”. In:
Control Engineering Practice 19(11):1363–1376 (2011).

[33] B. Verlaan. “An optimization based approach to autonomous drifting”. In:
Msc. Thesis at Delft University of Technology (2019).